INSTITUTE OF PHYSICS PUBLISHING JOURNAL OF PHYSICS: CONDENSED MATTER

J. Phys.: Condens. Matter **13** (2001) R235–R269 www.iop.org/Journals/cm PII: S0953-8984(01)13608-8

TOPICAL REVIEW

Spin-density waves in Fe/Cr trilayers and multilayers

R S Fishman

Solid State Division, Oak Ridge National Laboratory, Oak Ridge, TN 37831-6032, USA

Received 5 December 2000, in final form 1 January 2001

Abstract

This paper reviews the behaviour of spin-density waves (SDWs) in Fe/Cr trilayers and multilayers. After providing an overview of SDWs in bulk Cr, we discuss the predicted effects of SDWs on the exchange coupling of an Fe/Cr trilayer with perfect interfaces, which is nearly realized experimentally by a Cr wedge grown atop an Fe whisker and covered with a thin Fe film. While the observed phase slips in the exchange coupling are produced by transitions between collinear SDW phases with different numbers of nodes, the growth in the distance between phase slips with increasing temperature is attributed to a transition between incommensurate and commensurate SDWs. The theoretical consequences of Fe–Cr interdiffusion and interfacial steps at imperfect interfaces are then described. Whereas Fe–Cr interdiffusion causes the observed sign change in the exchange coupling, the effects of interfacial steps depend on which of the interfacial, magnetostatic, or bulk energies are dominant. For rough interfaces, the non-collinear coupling between the Fe moments can be explained by two competing models, one of which requires the formation of a non-collinear, helical SDW that is unstable in bulk Cr. Although both collinear and non-collinear SDWs have been directly observed in Fe/Cr multilayers with neutron scattering, the role of SDWs in the exchange coupling remains uncertain. This review focuses on the following open questions. Can a SDW be detected from the exchange coupling alone? What are the requirements for a non-collinear SDW in an Fe/Cr trilayer or multilayer? Can the proximity to a SDW instability be observed? Finally, what is the origin of the discrepancy between the observed exchange coupling and the much larger coupling predicted by phenomenological, tight-binding, and first-principles calculations?

1. Introduction

The role of the spin-density wave (SDW) within the Cr spacer of Fe/Cr trilayers and multilayers has been the subject of controversy since the first discoveries of antiferromagnetic (AF) coupling [1] and giant magnetoresistance (GMR) [2, 3] almost 15 years ago. It was originally assumed that SDWs play a central role in the observed short-period oscillation of the interlayer exchange coupling (IEC) between neighbouring Fe layers [4, 5]. But after the IEC was found to persist above the bulk Néel temperature of Cr [6] and other trilayers with non-magnetic

spacers were shown to exhibit similar short-period oscillations [7,8], some researchers [6,7,9] concluded that the SDW plays at most an incidental role in the IEC. Over time it has become clear that the truth lies somewhere in between: although not produced by the SDW, the IEC may be significantly changed by its presence.

Attention was first drawn to Fe/Cr trilayers by the observation in 1986 [1] that the Fe moments on either side of a Cr spacer were AF coupled for small Cr thickness. Due to its possible technological importance, a flurry of interest followed the discovery two years later [2, 3] that a modest magnetic field of a few kG produced a giant drop in the resistance (GMR) across the trilayer as the Fe moments became aligned. It was soon realized [10] that the magnetic coupling actually oscillates between AF and ferromagnetic (F) alignment of the Fe moments with a period of about 18 Å or 12.5 monolayers (ML). An early model [11] of the IEC in Fe/Cr trilayers predicted an additional coupling with a period close to 2 ML, which was believed to be hidden by surface roughness. The subsequent discovery [4,5] of this short-period coupling in an Fe/Cr trilayer with extremely clean interfaces was a triumph for exchange-coupling models.

The earliest analytic models [11, 12] of the IEC were based on RKKY theory for the interaction between d-band magnetic impurities (in the Fe layers) mediated by the wide-band electrons in a paramagnetic spacer. RKKY models dictated that the oscillation periods are directly related to the extremal wavevectors of the spacer's bulk Fermi surface (FS). The amplitudes of the exchange coupling were determined by quantum-well models [13–15], which treat the electrons in the spacer as particles placed in a quantum well between the potential barriers produced by the Fe layers. But neither RKKY nor quantum-well models consider the effects of a SDW, which produces an energy gap around the nested portions of the FS.

By contrast, tight-binding and first-principles techniques are well suited for studying the properties of a SDW in an Fe/Cr trilayer. For small N, tight-binding calculations [16, 17] indicated that a commensurate (C) SDW has lower free energy than the incommensurate (I) SDW which is stable in bulk Cr below $T_{\rm N}^{\rm bulk} \approx 311$ K. The earliest first-principles calculations [18] confirmed that an enhanced Cr moment is AF coupled to the Fe moment at the Fe–Cr interface. Recent first-principles calculations [19, 20] have verified that the SDW becomes incommensurate for N above about 25 ML.

Prior to 1995, the experimental techniques most commonly used to study Fe/Cr trilayers were scanning electron microscopy with polarization analysis (SEMPA), Brillouin light scattering (BLS), ferromagnetic resonance (FMR), and magneto-optic Kerr effect (MOKE) measurements. While none of these techniques can directly detect a SDW, several experiments suggested that SDWs play an important role in Fe/Cr trilayers. In a series of beautiful measurements [4, 21], the NIST group used SEMPA to image the exchange coupling through a Cr wedge, built atop an Fe whisker and overlaid with a thin Fe film. With each additional Cr layer, the IEC flips from F to AF and back again, but periodically undergoes a phase slip where the same magnetic coupling repeats. The distance between phase slips is 20 ML at room temperature and increases as the temperature is raised. Although the nodes of the bulk I SDW are separated by 27 ML at room temperature [22] and the phase slips persist well above $T_{\rm N}^{\rm bulk}$, the NIST group speculated that these phase slips were produced by an I SDW within the Cr spacer.

In 1995, the SDW in an Fe/Cr superlattice was directly observed for the first time with neutron scattering. Vindicating the speculations at NIST, measurements [23,24] on epitaxially grown multilayers detected a SDW both above and below $T_{\rm N}^{\rm bulk}$! But similar measurements [25, 26] on sputtered multilayers detected a SDW only above a critical thickness of 30 ML and below about 300 K. The disagreement between these two groups probably arises from the different conditions of the Fe–Cr interfaces in epitaxially grown and sputtered multilayers.

Ironically, many scientists lost interest in this system following the direct observation of SDWs by neutron scatterers. Yet experiments have demonstrated that the SDWs in Fe/Cr multilayers display a rich variety of behaviour. In epitaxially grown multilayers, for example, the Fe–Cr interaction stabilizes [24] a non-collinear, helical (H) SDW which is unstable in bulk Cr alloys. Since the SDW phase can be controlled by simply flipping the Fe moments, Fe/Cr superlattices provide a laboratory for exploring the physics of itinerant antiferromagnetism.

Despite the experimental evidence for SDWs in Fe/Cr superlattices, the effect of a SDW on the IEC is still an open question. This question can be rephrased: 'If stranded on a desert island without neutron-scattering facilities but with BLS and MOKE apparatus available, could you detect a SDW in the spacer of a magnetic multilayer?' Keeping in mind that a negative response would relegate SDWs to a merely decorative role, our answer is happily yes: SDWs can be detected by the dependence of the IEC amplitude and wavevector on thickness and temperature. This review discusses several other open questions such as under what conditions non-collinear SDWs are stabilized in an Fe/Cr trilayer or multilayer, the role of non-collinear SDWs in the possible non-linear coupling between the Fe moments, and finally, the origin of the disagreement between the observed bilinear (BL) exchange coupling and the much larger coupling predicted theoretically.

In the following section, we provide a brief overview of SDWs in bulk Cr. Section 3 is devoted to 'perfect' trilayers without interfacial disorder, a system which is closely realized by an Fe/Cr wedge. After examining the theoretical models and measurements of the BL exchange coupling, we discuss the conditions for a non-collinear SDW in a perfect trilayer. In section 4, we study the consequences of Fe–Cr interdiffusion and interfacial steps. We also review the predictions of two competing models for the non-collinear coupling between the Fe moments. In the final section, we return to the open questions posed above.

There are already several excellent reviews on Fe/Cr superlattices. In particular, we direct the reader to the review by the NIST group [27] on SDWs in wedges and multilayers, with an emphasis on experimental techniques commonly available on desert islands. For a perspective which emphasizes neutron scattering, consult the recent review by Zabel [28]. The two comprehensive reviews by Fawcett and Fawcett *et al* [22] are recommended to the reader interested in bulk Cr and its alloys. Because they were the first to attract interest, Fe/Cr trilayers are treated by many of the seminal theoretical works on the IEC in trilayers with paramagnetic spacers, a field which was recently reviewed by Stiles [29] and Bruno [30]. Considering this plethora of reviews, the reader may wonder why another is needed. As alluded to above, the present review takes a somewhat different perspective to those just mentioned by focusing on the role of SDWs in the IEC.

2. SDWs in bulk Cr

Antiferromagnetism in bulk Cr is produced by the Coulomb attraction between electrons and holes on nearly nested portions of the FS [31–33]. A two-dimensional slice [34] of the FS of bulk, body-centred cubic Cr is sketched in figure 1. The electron jack centred at the Γ point and the hole octahedra centred at the H points are roughly nested by three sets of nesting wavevectors, of which we have drawn the set $\boldsymbol{Q}_{\pm}$ along the $\hat{z}$-axis. The selected H and Γ points are joined by half of the reciprocal-lattice vector $\boldsymbol{G}_z = (4\pi/a)\hat{z}$, where a is the lattice constant for the conventional cubic unit cell. Because the hole octahedron is slightly larger than the electron jack, the nesting wavevectors can be written as $\boldsymbol{Q}_{\pm} = (\boldsymbol{G}_z/2)(1 \pm \delta)$, where the FS mismatch δ is about 0.05 for pure Cr. Also of importance for future discussion are the hole ellipses centred at the N points and the lenses across the necks of the electron jack.

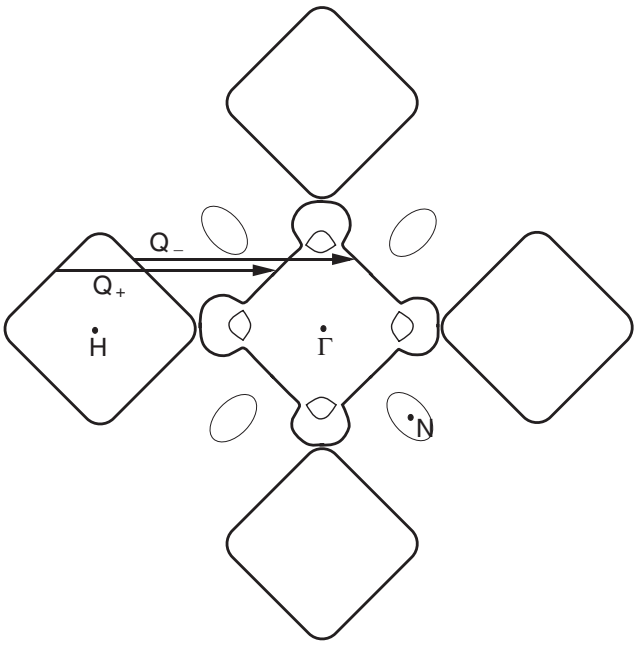

Figure 1. A two-dimensional slice of the Fermi surface of bulk Cr, showing the electron jack centred at the Γ point, the hole octahedron centred at the H points, hole ellipses at the N points, and one set $\boldsymbol{Q}_{\pm}$ of nesting wavevectors.

In order to maximize the electron–hole coupling between both left and right faces of the hole octahedron and electron jack, the SDW develops not at the nesting wavevectors $\boldsymbol{Q}_{\pm}$ but rather at the ordering wavevectors $\boldsymbol{Q}'_{\pm} = (\boldsymbol{G}_z/2)(1 \pm \delta')$, which are slightly closer to $\boldsymbol{G}_z/2$ with $0 \leqslant \delta' < \delta$ [35]. Whereas δ is fixed by the FS topology, δ' is obtained by minimizing the nesting free energy. Consequently, δ depends only weakly on temperature with energy scale $\epsilon_{\mathrm{F}} \approx 7$ eV [36] while δ' depends much more sensitively on temperature with energy scale $T_{\mathrm{N}}^{*} \approx 100$ meV.

When $\delta' = 0$, the SDW with wavevector $\boldsymbol{G}_z/2$ corresponds to the C SDW drawn in figure 2 with the spin having the same magnitude at every site. When $\delta' > 0$, two types of SDW are possible: a collinear I SDW and a non-collinear H SDW, both pictured in figure 2. For the I SDW, $1/\delta'$ is the number of ML between nodes; for the H SDW, $1/\delta'$ is the distance in ML for a π-twist of the helix. Since neighbouring ML lie a distance $a/2$ apart, both I and H SDWs have period a/δ'. Due to the presence of nodes, an I SDW cannot be created from a C SDW. But a H SDW can be smoothly generated from a C SDW by simply twisting one end.

Both δ and δ' may be controlled by doping. Doping with either Mn or Fe, which have more electrons than Cr, raises ϵ_{F} and decreases δ. Simultaneously, the Néel temperature $T_{\mathrm{N}}^{\mathrm{bulk}}$ increases, δ' decreases, and the I SDW period grows. Below some critical, non-zero value of δ, δ' vanishes and the SDW becomes commensurate. About 0.2% Mn or 2.4% Fe are required to achieve this condition. With further Mn or Fe doping, δ continues to decrease and $T_{\mathrm{N}}^{\mathrm{bulk}}$ continues to rise. By comparison, V has fewer electrons than Cr so doping with V lowers ϵ_{F} and increases δ. Correspondingly, $T_{\mathrm{N}}^{\mathrm{bulk}}$ decreases, δ' increases, and the I SDW period shrinks. At a critical value of about 4% V, $T_{\mathrm{N}}^{\mathrm{bulk}}$ vanishes [22].

Because the Bloch wavefunctions of the d-band electrons which comprise the SDW are strongly peaked at the lattice sites $\boldsymbol{R}$, the three varieties of SDW propagating in the z-direction

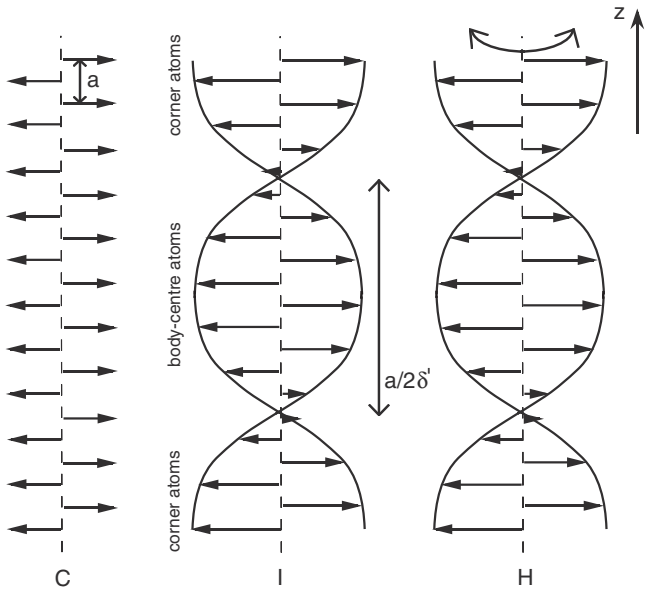

Figure 2. The bulk C, I, and H SDWs. For the I SDW, the T state is drawn for simplicity. In the L state, the moments would lie along the z-axis. For the H SDW, the moments are projected onto the page.

can be written as

$$\boldsymbol{S}_{\mathrm{Cr}}(R_z) = (-1)^{2R_z/a}\hat{\boldsymbol{m}}\alpha_s g(T)\cos(\theta) \qquad \text{C SDW} \qquad (1)$$

$$\boldsymbol{S}_{\mathrm{Cr}}(R_z) = (-1)^{2R_z/a}\hat{\boldsymbol{m}}\alpha_s g(T)\cos\bigl((2\pi/a)\delta' R_z + \theta\bigr) \qquad \text{I SDW} \qquad (2)$$

$$\boldsymbol{S}^{(\pm)}_{\mathrm{Cr}}(R_z) = (-1)^{2R_z/a}\alpha_s g(T) \times\Bigl\{\hat{\boldsymbol{x}}\cos\bigl((2\pi/a)\delta' R_z + \theta\bigr) \pm \hat{\boldsymbol{y}}\sin\bigl((2\pi/a)\delta' R_z + \theta\bigr)\Bigr\} \qquad \text{H SDW} \qquad (3)$$

where α_s is a constant, $\hat{\boldsymbol{m}}$ is an arbitrary polarization, and $g(T)$ is a temperature-dependent order parameter. Although θ is arbitrary in the I state, $\theta = \pi/4$ is fixed by charge conservation in the C state [37]. So the amplitudes of the C and I SDWs are given by $\alpha_s g(T)/\sqrt{2}$ and $\alpha_s g(T)$, respectively. Across a second-order IC phase transition with the same order parameter g on both sides, the SDW amplitude drops by a factor of $1/\sqrt{2}$ but the rms value $\alpha_s g/\sqrt{2}$ is continuous. For a right- or left-handed H SDW, the spin on each site is equal to the amplitude of an I SDW with the same order parameter g.

Depending on whether the spin polarization $\hat{\boldsymbol{m}}$ is perpendicular or parallel to the ordering wavevectors along the z-axis, the I SDW of equation (2) is either transverse (T) or longitudinal (L). In the T phase, there are two possible SDWs (with perpendicular polarizations) for each set of ordering wavevectors $\boldsymbol{Q}'_{\pm}$. On the other hand, a C SDW depends only on the polarization direction $\hat{\boldsymbol{m}}$ and not on the orientation of the ordering wavevector.

Pure Cr undergoes a Néel transition at $T_{\mathrm{N}}^{\mathrm{bulk}} = 311$ K into a transverse, I SDW phase (which we shall call the T SDW state). Below the spin-flip temperature of $T_{\mathrm{SF}} = 123$ K, the T SDW state transforms into a longitudinal, I SDW state (called the L SDW state) [22]. At low temperatures, the rms moment of pure Cr is about $0.4\mu_{\mathrm{B}}$, corresponding to an amplitude of about $0.6\mu_{\mathrm{B}}$.

The free-energy difference ΔF between the SDW and paramagnetic (P) phases can be constructed by applying the random-phase approximation to a Hamiltonian containing the

Coulomb interaction U between electrons and holes on the nested Fermi surfaces, which are modelled as octahedra of different sizes [33,35,38]. Remarkably, U only enters ΔF implicitly through $T_N^* \approx 100$ meV, which is the Néel temperature for a perfectly nested Cr alloy with $\delta = 0$. Since T_N^* neglects the effects of impurity scattering, the actual Néel temperature is always smaller than this value. Doping enters the free energy through the energy mismatch $z_0 = 4\pi\delta v_F/\sqrt{3}a$ between the nested Fermi surfaces. While V impurities increase z_0, Mn or Fe impurities lower z_0. In units of T_N^*, the triple point where the P, C, and I phases meet is given by $z_0 = 4.3T_N^*$ [38]. Pure Cr is believed to have an energy mismatch of about $z_0 = 5T_N^*$.

Minimizing the free energies $\Delta F_I(g, \delta', T, z_0)$ and $\Delta F_H(g, \delta', T, z_0)$ of the I and H phases with respect to g and δ' yields the bulk values for the SDW amplitude and wavevector. Although the H SDW was the first SDW predicted by Overhauser [31], it has higher free energy than an I SDW with the same T and z_0 and has never been observed in bulk Cr alloys. Nevertheless, the local H SDW minimum of the nesting free energy has important consequences for the magnetic order of Fe/Cr trilayers. The free energy $\Delta F_C(g, T, z_0)$ of a C SDW can be obtained from either ΔF_I or ΔF_H in the limit $\delta' \to 0$. In a first-order transition between I and C phases with a discontinuous change in δ', the C phase compensates for the loss of nesting with an enhanced order parameter g. For this reason, the low-temperature, rms moment jumps from about $0.4\mu_B$ to $0.8\mu_B$ across the IC transition in CrMn or CrFe alloys [22].

Since it is produced by bound electron–hole pairs, a SDW generates an energy gap in the quasiparticle spectrum [39, 40] of the nested electron jack and hole octahedron. Keep in mind that the total, single-spin density of states (DOS) of Cr is estimated to be between 2 and 4 times larger than the single-spin DOS ρ_{eh} of the two nested FSs [36], so the SDW only destroys between 1/2 and 1/4 of the FS. The remainder of the FS, including the ellipses and lenses mentioned earlier, are ungapped and still contribute to the electronic conductivity below T_N^{bulk}. While the gapped portion of the FS is primarily d in character, the ungapped portions are primarily s and p in character.

Bulk Cr alloys are known [22] to be highly sensitive to magnetoelastic effects. Qualitatively, applying pressure to a Cr alloy has the same effect as increasing the mismatch energy z_0: any C SDW is destabilized, the I SDW period shrinks, and the Néel temperature drops. Near T_N^{bulk}, the observed change in the SDW period is described by the empirical relation $\Delta Q'_+/Q'_+ = -0.54 \times 10^{-6}$ bar^{-1} ΔP. Recently, Marcus *et al* [41] noted that the observed volume expansion of 0.8% below T_N^{bulk} is required to stabilize the SDW in pure Cr. By compromising the stability of the SDW, compression of the lattice by pressure or strain suppresses the Néel temperature and the SDW amplitude.

In the next section, we argue that the observed phase-slip distance of 20 ML at room temperature [21] corresponds to the distance between SDW nodes within the Cr spacer. But the distance between SDW nodes in bulk Cr is 27 ML at room temperature. Can the 0.6% lattice mismatch between Fe and Cr explain this apparent suppression of the SDW period? Using the relationship [42] between ΔP and the lattice strain, we find that a compressive strain of only 0.26% in the x- and y-directions extending throughout the Cr spacer would produce a 25% reduction in the SDW period! Considering that the lattice strain is closest to 0.6% at the bottom of the Cr wedge near the Fe whisker, this is a very reasonable result. The effect of lattice strain on an Fe/Cr wedge can be modelled using a mismatch energy of $z_0 = 6.4T_N^*$, which produces an I SDW with period close to 40 ML at $T_N^{bulk}(z_0)$ (which is now smaller than the Néel temperature of pure Cr due to the larger FS mismatch).

We also wish to emphasize that the magnetic susceptibility χ of a SDW depends on whether the moments are parallel or perpendicular to the applied field $\boldsymbol{H}$. As in a local-moment antiferromagnet, $\chi^\perp > \chi^\parallel$, so a magnetic field tends to align the SDW moments perpendicular to $\boldsymbol{H}$ [43].

3. SDWs in 'perfect' trilayers

This section considers the properties of an Fe/Cr trilayer with perfect interfaces. Surprisingly, the notion of a perfect interface is not so far-fetched. The small lattice mismatch between (100) Fe and Cr permits very good epitaxial growth. Perhaps more importantly, Fe whiskers are among the most atomically flat materials known to exist. Therefore, a Cr wedge grown on an Fe whisker and covered with a thin Fe film can be made to very exacting standards. While some Fe–Cr interdiffusion and surface roughness are inevitable, their effects are easily isolated. After reviewing the theoretical models for a perfect Fe/Cr trilayer, we describe the results of SEMPA, MOKE, and BLS measurements. Finally, we discuss the conditions for non-collinear SDWs in a perfect Fe/Cr trilayer.

3.1. Theory of the IEC and collinear SDWs in trilayers

Unlike the SDW in bulk Cr, the SDW in a Cr spacer may contain several non-harmonic components. In a trilayer with spacer thickness N and z-axis perpendicular to the planes, the spin modulation may be written as

$$\boldsymbol{S}_{\mathrm{Cr}}^{(N)}(R_z) = \hat{\boldsymbol{m}} \sum_n C_{N,n} \cos\bigl(Q_{N,n} R_z + \theta_{N,n}\bigr) \tag{4}$$

which reduces to the bulk results when $Q_{N,n} = Q'_{\pm}$, $\theta_{N,n} = \theta$, and $C_{N,n} = \alpha_s g(T)$. For simplicity, the polarizations $\hat{\boldsymbol{m}}$ of each of the components are assumed to be the same. Likewise, the energy difference J_{c} between AF and F orientations of the Fe moments in a spacer of width L may also be written as a superposition:

$$J_{\mathrm{c}}(L) = \sum_n D_{L,n} \sin\bigl(q_n L + \psi_n\bigr). \tag{5}$$

The models discussed below attempt to evaluate the amplitudes, wavevectors, and phases of the IEC parametrized in equation (5).

Theories of the IEC and collinear SDWs in Fe/Cr trilayers can be roughly divided into four classes. Phenomenological models are convenient for studying the competition between SDW phases as a function of temperature and spacer thickness. Although tight-binding models provide a more realistic description of the moments near the interfaces and within the Fe layers, they are in practice restricted to zero temperature and to relatively small Cr spacers. Because they treat the spacer as paramagnetic, RKKY and quantum-well models can be used to isolate the effects of FS topology from the effects of the SDW. First-principles calculations are the most rigorous models considered but they have only recently attained the computing power needed to study relatively large Cr spacers.

3.1.1. Phenomenological models. The phenomenological model developed by Shi and Fishman [44–46] assumes that the AF interfacial Fe–Cr interaction may be written as $J_i \boldsymbol{S}_{\mathrm{Fe}}^{\mathrm{I,II}} \cdot \boldsymbol{S}_{\mathrm{Cr}}(z)$ at interfaces I ($z = a/2$) or II ($z = Na/2$) with exchange-coupling constant $J_i > 0$ (more about this in a moment). In addition, the Fe moments are assumed to be either F or AF aligned with $\boldsymbol{S}_{\mathrm{Fe}}^{\mathrm{I}} = \boldsymbol{S}_{\mathrm{Fe}}^{\mathrm{II}}$ or $\boldsymbol{S}_{\mathrm{Fe}}^{\mathrm{I}} = -\boldsymbol{S}_{\mathrm{Fe}}^{\mathrm{II}}$, both in-plane. The SDW will then be transversely polarized with respect to the ordering wavevectors along the z-axis. Combining the interfacial energies with the SDW free energy in a spacer of width $L = (N-1)a/2$, the free energy of a trilayer per interfacial area a^2 becomes

$$E = J_i \bigl\{ \boldsymbol{S}_{\mathrm{Fe}}^{\mathrm{I}} \cdot \boldsymbol{S}_{\mathrm{Cr}}(a/2) + \boldsymbol{S}_{\mathrm{Fe}}^{\mathrm{II}} \cdot \boldsymbol{S}_{\mathrm{Cr}}(Na/2) \bigr\} + \Delta F_{\mathrm{I}} L a^2 \tag{6}$$

where $\boldsymbol{S}_{\rm Cr}(R_z)$ is either a collinear C or I SDW with order parameter g and period a/δ' independent of z. In other words, the SDW is assumed to be rigid with only a single Fourier component.

As discussed shortly, both tight-binding and first-principles methods imply that the SDW loses its rigidity within a couple of ML from each Fe–Cr interface, where the Cr moments are enhanced. That conclusion also follows from the electron–hole coherence length [47] of the SDW $\xi_0 \sim \hbar v_{\rm F}/\pi g$, which is of order 10 Å. Hence, both g and δ' are expected to be modified within a few ML from each interface.

Clearly, the interfacial energies in equation (6) favour placing the SDW antinodes near the Fe–Cr interfaces. Due to the assumed rigidity of the SDW, the interfacial energies always induce some degree of SDW order with $g > 0$ throughout the spacer no matter how high the temperature. Hence, the P state is never stable and the Néel temperature $T_{\rm N}^{\rm lay}$ of the trilayer is infinite within this model.

After fixing the magnetic orientations of the Fe moments to be F or AF, the SDW amplitude g, periodicity $1/\delta'$, and phase θ are chosen[1] to minimize the energy E in equation (6). The corresponding F and AF energies of the trilayer are denoted by $E_{\rm F}$ and $E_{\rm AF}$, which depend only on the dimensionless coupling strength $\gamma = J_i\alpha_s S_{\rm Fe}/(V/N)\rho_{\rm eh}T_{\rm N}^*$. A value of $\gamma = 3$ corresponds to an Fe–Cr exchange interaction J_i of 7 meV.

Strictly speaking, a one-to-one correspondence cannot be made between itinerant and local-moment models, a point which is driven home by the non-half-integer and spatially dependent spin of an I SDW. So it is not really proper to associate effective exchange couplings with the Fe–Fe, Fe–Cr, and Cr–Cr interactions. Nonetheless, a great deal of useful insight can be gained by making connections with local-moment models. The estimate given above for the Fe–Cr exchange coupling is only slightly smaller than the estimate $J_i \approx 10$ meV made by Bödeker *et al* [48], based on the classical Heisenberg model. By contrast, this value is about ten times smaller than the estimate made by Berger and Fullerton [49], based on a similar fit.

From $E_{\rm AF}$ and $E_{\rm F}$, Shi and Fishman [44] evaluated $J_{\rm c} = E_{\rm AF} - E_{\rm F}$ as a function of temperature T and thickness L. Taking $\gamma = 3, z_0/T_{\rm N}^* = 5, (V/N)\rho_{\rm eh} = 3.7$ states Ryd^{-1}/atom [36], and $T = 0.5T_{\rm N}^{\rm bulk}$ or $1.2T_{\rm N}^{\rm bulk}$, the authors obtained the results in figure 3 for $J_{\rm c}(N)$. As expected, $J_{\rm c}$ oscillates between F ($J_{\rm c} > 0$) and AF ($J_{\rm c} < 0$) values with a short 2 ML period. Below $T_{\rm N}^{\rm bulk}$ in figure 3(a), $J_{\rm c}$ decays slowly with short-period amplitude $D_{L,s} \propto 1/L^{1/2}$. Above $T_{\rm N}^{\rm bulk}$ in figure 3(b), $J_{\rm c}$ falls off more rapidly with $D_{L,s} \propto 1/L^2$.

For $N < 28$, figure 3(a) indicates that the stable orientation of the Fe moments at low temperatures is F for odd N and AF for even N. This coupling then alternates between F and AF until the phase slip at $N = 28$. For both $N = 27$ and $N = 28$, the stable orientation is F. Until the next phase slip at $N = 46$, the stable orientation is F for even N and AF for odd N. With each phase slip, the number of SDW nodes $n \approx (N-1)\delta'$ increases by one. So the SDW is commensurate prior to the first phase slip, contains one node for $28 \leqslant N \leqslant 45$, and two nodes for $46 \leqslant N \leqslant 71$.

These results are recast in figures 4(a) and 4(b), which plot the magnetic phase diagram for unstrained ($z_0 = 5T_{\rm N}^*$) and strained ($z_0 = 6.4T_{\rm N}^*$) Cr spacers. Also displayed are the numbers n of SDW nodes in the stable phase. The thick solid curve denotes the IC transition while the thinner curves denote the transitions between I phases with different n, which coincide with the phase slips. Notice that a SDW is stabilized by the Fe–Cr interfacial energies even above the bulk Néel temperature and that the C phase is stable for small N or high T.

[1] This implicitly assumes that the SDW amplitudes rather than the rms moments are equal near the Cr–Fe interface in I and C phases with the same order parameter g [45]. For the C phase, charge conservation [37] then requires that between 0.005 and 0.014 electrons per Cr atom are transferred from the Fe layers to the Cr spacer within a coherence length ξ_0 from the interface.

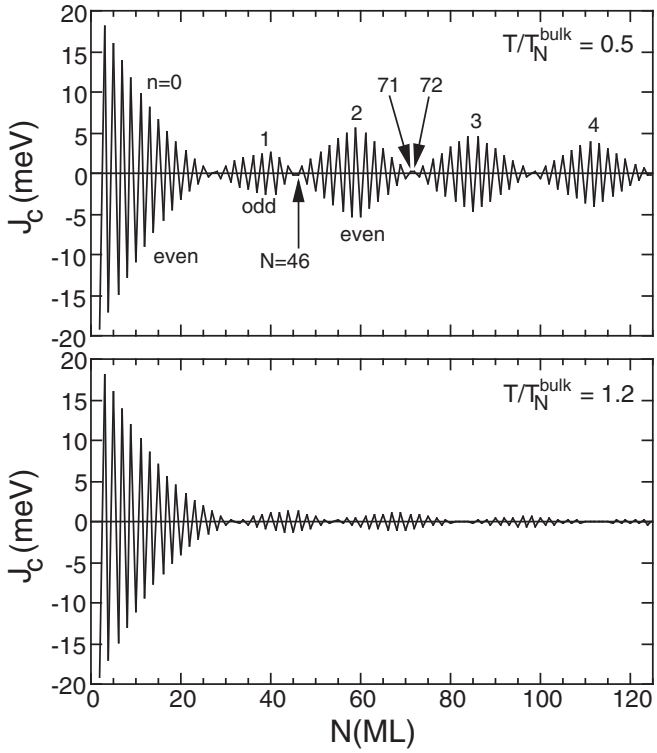

Figure 3. The IEC in meV as a function of the spacer thickness for $z_0/T_N^* = 5$, $\gamma = 3$, and (a) $T = 0.5T_N^{bulk}$ or (b) $T = 1.2T_N^{bulk}$ [46].

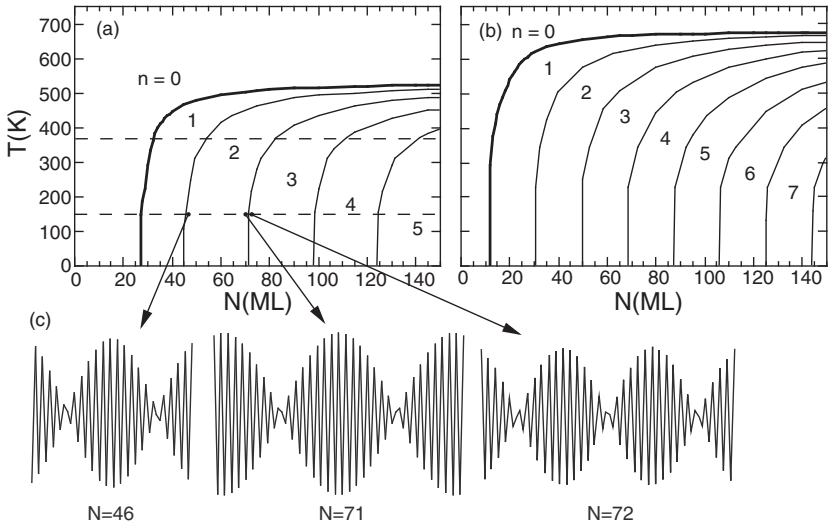

Figure 4. The phase diagram of Fe/Cr multilayers and wedges for $\gamma = 3$ and (a) $z_0 = 5T_N^*$ or (b) $z_0 = 6.4T_N^*$. The thick solid curve denotes the IC transition while the thin solid curves separate different I phases with n nodes [45]. (c) The SDW for three values of the spacer thickness, $z_0 = 5T_N^*$, and $T/T_N^{bulk} = 0.5$ (lower dashed line in (a)).

Returning to figures 3(a) and 3(b), phase slips occur whenever a thin solid curve in figure 4(a) is crossed at $T = 0.5T_N^{bulk}$ or $1.2T_N^{bulk}$ (along the dashed lines). As the temperature increases, the phase boundaries are shifted to the right and further apart. Both above and below the bulk Néel temperature, the phase slips are very regularly spaced. Below T_N^{bulk}, the phase-slip distance is close to the node-to-node distance of the bulk SDW and rigorously approaches this distance as $N \to \infty$. As $T \to T_{IC}$, the distances between phase slips diverge as the SDW becomes commensurate.

As anticipated, the bulk Néel temperature $T_N^{bulk} \approx 230$ K of the strained Cr spacer in figure 4(b) is suppressed compared to that of unstrained Cr. But the large-N limits of T_{IC} for the unstrained and strained Cr spacers are 525 and 675 K, respectively. So $T_{IC}(N \to \infty)$ increases with the FS mismatch. This result is not difficult to understand: as the mismatch increases, the I SDW free energy decreases with respect to the C SDW free energy even when the I and C SDWs are stabilized by the interfacial energies. Fishman and Shi [45] found that T_{IC} increases almost linearly with z_0 and intersects the bulk Néel temperature at the triple point.

The dependence of the SDW amplitude and wavevector on thickness was discussed in reference [44]. With increasing N, both g and δ' approach their bulk values ($g \sim 1/N$ above T_N^{bulk}) and the oscillations about the bulk values become narrower. As N increases between phase slips, the number of SDW nodes remains the same but the SDW stretches to maximize the AF coupling at the interfaces. Except midway between phase slips, when N is a multiple of the bulk value of $1/\delta'$, the SDW antinodes are slightly displaced from the interfaces. When n increases by one, the SDW period suddenly contracts with the addition of another node and the SDW amplitude decreases discontinuously. This behaviour is portrayed by the SDWs in figure 4(c) for the same parameters as used in figure 3(a).

A C SDW is predicted to be stable for small spacer thicknesses or high temperatures. In both regimes, the free-energy difference $\Delta F_I L$ between the ordered and P phases is small and the interfacial energy dominates. The interfacial energy is minimized when the number of SDW nodes satisfies $n = 2m + 1 + N$ for F coupling or $n = 2m + N$ for AF coupling, with integer m and $\delta' = n/(N-1)$. So for F coupling with even (odd) N, the SDW must contain an odd (even) number of nodes whereas for AF coupling with even (odd) N, the SDW must contain an even (odd) number of nodes. When the interfacial energy is minimized, the total free energy is given by $E = -2J_i\alpha_s g S_{Fe} + \Delta F_I(g, \delta')\, La^2$. Recall that for C ($\delta' = 0$) and I ($\delta' \geqslant 1/(N-1)$) phases with the same free energy ΔF_I, the C phase has the larger order parameter g. It follows that the C SDW has a lower free energy than the I SDW for sufficiently small N or high T. Of course, the stability of the C phase requires that the Fe moments can freely switch from F (odd N) to AF (even N). We shall refer to this condition as commensurate friendly (CF). When the Fe moments are non-CF (F for even N or AF for odd N), the SDW must be incommensurate with an odd number of nodes.

3.1.2. Tight-binding models. Unlike the phenomenological model just described, real-space tight-binding models make no assumptions about the form of the Cr or Fe moments. In practice, however, these models are restricted to Cr spacers smaller than 30 ML and to $T = 0$. The first tight-binding calculations by Victora and Falicov [50] for a single ML of Cr on Fe(100) indicated that the Cr and Fe moments are AF coupled with an enhanced Cr moment of $3.6\mu_B$. Applying the tight-binding method to Fe/Cr trilayers with Cr spacers of 5 ML or less, Hasegawa [51] found that the Cr moments are suppressed when the Fe moments are non-CF but he did not provide a detailed calculation of $J_c(L)$.

Much more extensive tight-binding calculations for Fe/Cr trilayers were performed by Stoeffler and Gautier [16, 17]. For small N, those authors concluded that the C and I phases are stable under CF and non-CF conditions, respectively. As seen in figure 5, the Cr moment

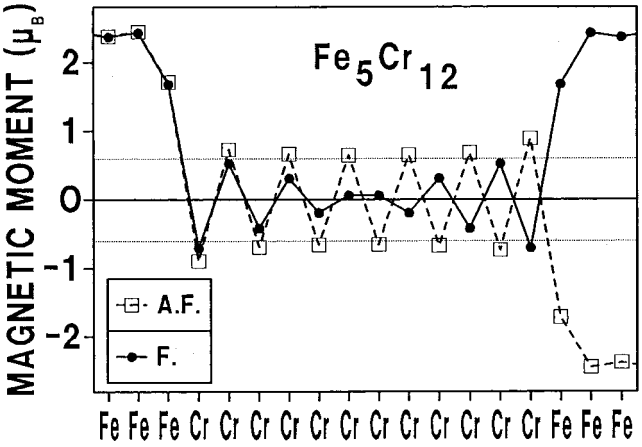

Figure 5. The SDW configurations in an Fe_5/Cr_{12} trilayer for F (full line) and AF (dashed line) coupling [17].

is enhanced within a couple of ML from the interface, but this enhancement is not nearly as large as predicted by Victora and Falicov [50] for a single ML. By comparison, the interfacial Fe moment is reduced from its bulk value. This can be explained by the hybridization of the Cr and Fe d bands whereby the Cr band narrows and the Fe band widens.

Stoeffler and Gautier emphasized that the free energy of the I phase is higher than that of the C phase due to the energy cost of a 'defect' or node in the SDW. Therefore, the exchange energy plotted in the solid curve of figure 6 always favours CF conditions. Notice that the magnitude of the IEC is just slightly larger than later found by Shi and Fishman [44].

3.1.3. RKKY and quantum-well models. Because they treat the spacer as paramagnetic, RKKY and quantum-well models are not of direct relevance to Fe/Cr trilayers. However, many of these models were originally developed for an Fe/Cr trilayer with a non-magnetic Cr spacer, i.e. a spacer with the same FS topology as Cr but without the Coulomb interaction responsible for the bulk SDW. Consequently, these models are useful for distinguishing whether exchange properties come from the FS topology or from the SDW instability.

RKKY models are based on the work of Yafet [52] for the exchange coupling across a one-dimensional electron gas. The period of the IEC was predicted to be inversely proportional to the Fermi momentum k_F of the gas. Subsequently, Wang *et al* [11] realized that the nesting property of the bulk Cr FS produces a short-period, 2 ML oscillation in Fe/Cr trilayers. Even a small degree of Fe–Cr intermixing disrupts this short-period oscillation, which explains its absence from experimental measurements made up to that time. This group [11, 53–55] also argued that the predominance of AF coupling for small N is caused by the superexchange interaction, which is enhanced by a peak in the Cr DOS just above ϵ_F.

Unlike RKKY models, quantum-well models [12–14] are non-perturbative and have been used to evaluate the amplitudes $D_{L,n}$ as well as the wavevectors q_n of the IEC. The earliest such models [14] assumed that the majority d bands in both the magnetic and spacer layers were perfectly matched while the band offset confined the minority electrons within the spacer. Over time, these models have become increasingly sophisticated and, as discussed further in section 5, provide very accurate predictions for trilayers with non-magnetic spacers. The predicted quantum-well states were directly observed in photoemission measurements [56,57] on Co/Cu trilayers.

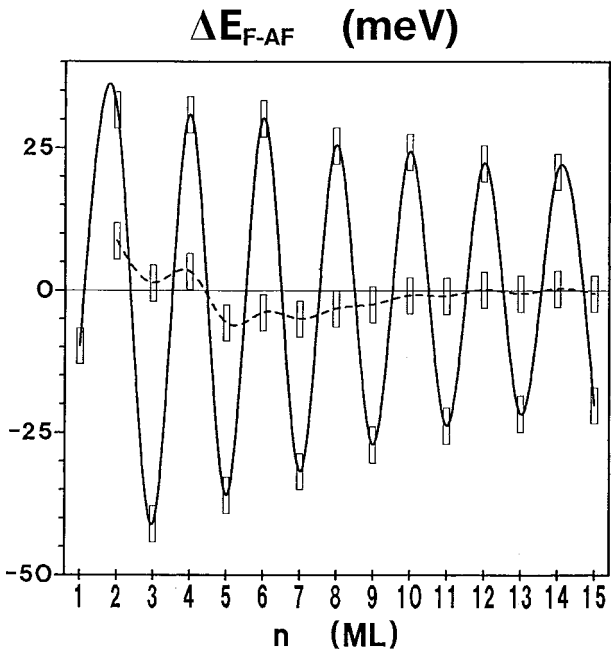

Figure 6. The IEC (note the change in sign compared to our convention) as a function of spacer thickness for an Fe_5Cr_n trilayer [17]. Rectangles give an estimate of the error. See the text for further explanation.

Both RKKY and quantum-well models obtain the IEC wavevectors from the calipers or extremal wavevectors of the bulk FS [58], suitably modified to account for the discrete spacing of the atoms [12]. Quantum-well models dictate that the wavevectors q_n with the largest amplitudes $D_{L,n}$ in equation (5) are associated with the maximum contrast between the confinement of the majority and minority electrons in the spacer layer [15, 59]. In Fe/Cr trilayers, the short-period coupling with predicted wavevector $q_s = Q_\pm$ and period $2/(1-\delta) \approx 2.1$ ML is produced by the nesting between the electron jack and hole octahedron in figure 1. There is still some lingering uncertainty over the origin of the long-period coupling of 18 Å. This nearly isotropic coupling [60] probably arises from the ellipses centred at the N points in figure 1 [59, 61] but could also come from the lenses of the electron jack [62, 63].

Several predictions of quantum-well models are important to the forthcoming discussion. For a FS caliper joining two points, D_L is predicted to decay like $1/L^2$ at $T = 0$. Partial nesting is believed to cause a $1/L^{3/2}$ decay whereas complete nesting such as in Cr causes a $1/L$ decay [12]. Based on the precise shape of the nested FSs in Cr, recent calculations [64] predict a $1/L^{3/2}$ decay of the short-period coupling at $T = 0$. At non-zero temperatures, D_L is found [65] to decay more rapidly than at zero temperature. Whereas the wavevector and phase of the coupling are independent of T, the amplitude D_L is proportional [14] to $T/\sinh(2\pi T/\hbar\omega_c)$, where $\omega_c = v_F/2L$ is the effective cyclotron frequency. This temperature dependence has been verified in Co/Ru trilayers [66]. Using the Fermi velocity $v_F = 2500$ meV Å of the octahedral FSs in bulk Cr, quantum-well models yield a temperature scale $\hbar\omega_c/2\pi$ of roughly[2] 1500 K/N.

[2] Within the quantum-well model, this temperature scale governs the short-period coupling. For the long-period coupling, v_F must be given by the Fermi velocity of the FS ellipses or lenses, which is probably much larger than the Fermi velocity of the nested electron jack and hole octahedron.

3.1.4. First-principles calculations. Finally, we consider first-principles calculations which are most commonly performed using the local spin-density approximation (LSDA). Rather than go into much detail about each such calculation, for example about the basis set, we invite the interested reader to look up the individual references. Using what is called the force theorem or the frozen-potential method [67], each calculation evaluates the difference between the F and AF energies from the change in the sum of single-particle energies. The non-self-consistent and frozen bulk potentials in the Fe and Cr layers [68] are taken to be the same for each magnetic orientation. Before weighing the significance of the LSDA calculations described below, the reader must be forewarned that such calculations have experienced difficulties in obtaining the SDW ground state of bulk Cr [41, 69].

Levy *et al* [70] performed the first LSDA calculations for an Fe/Cr trilayer, with the by-now-expected result that the Cr moments are enhanced (but still somewhat smaller than their bulk values) when the Fe moments are CF. Assuming that the I SDW antinodes lie precisely at the Fe–Cr interfaces, van Schilfgaarde and Herman [71] obtained a C SDW for $N < 21$, an I SDW with a single node for $N \geqslant 22$, and a phase slip joining the two. For thicknesses above 21 ML, the predicted exchange coupling had periods of 2.05 and 12.3 ML. While the short-period amplitude $D_{L,s}$ was independent of L, the long-period amplitude $D_{L,l}$ decayed like $1/L^2$. The magnetic coupling produced by the SDW overwhelmed the RKKY coupling obtained in the absence of SDW order.

First-principles calculations by Mirbt *et al* [72, 73] were used to isolate the effect of the Coulomb interaction U in an Fe/Cr trilayer with semi-infinite Fe layers. As shown in figure 7, the Fe–Cr interaction induces a spin modulation in the Cr spacer even when $U = 0$ [73]. But the Cr moments are about 20 times larger when $U > 0$. Although J_c has a 2 ML period in either case, $D_{L,s}$ is twice as large when $U > 0$. For non-CF Fe moments, an I spin modulation is produced for both $U = 0$ and $U > 0$. The close agreement between these predictions and experiments implies [72] that an AF superexchange interaction [11] is not required to explain the exchange coupling in Fe/Cr trilayers. Keep in mind, however, that even when $U > 0$ these LSDA calculations do not support the formation of a bulk SDW.

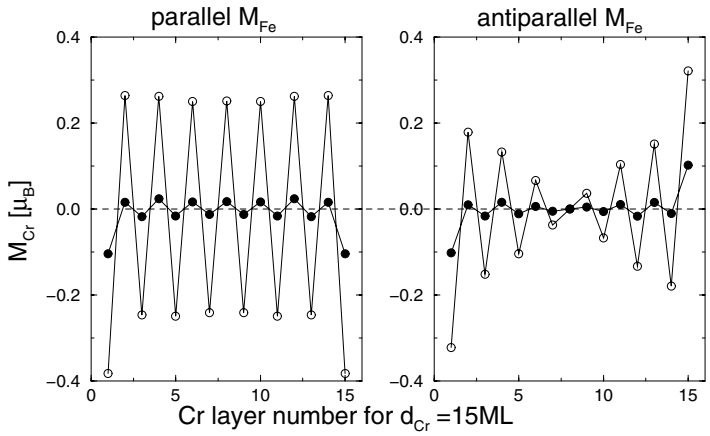

Figure 7. Magnetic moments in a Cr spacer with $U = 0$ (dark circles) or $U > 0$ (open circles) and F (left) or AF (right) Fe moments, both with $N = 15$ [73].

Recently, the computational power required to study larger Cr spacers has become available. Both Hirai [19] and Niklasson *et al* [20] studied the development of an I SDW at $T = 0$. Hirai concluded that if the lattice constant of an Fe/Cr multilayer is chosen to minimize

the total energy for each N, a C-to-I transition occurs between 9 and 19 ML. Niklasson *et al* did not achieve the resolution required to evaluate the IEC. However, they did evaluate the SDW amplitudes and wavevectors in equation (4) for a fixed alignment of the Fe moments in an Fe/Cr trilayer. As expected, the I SDW has antinodes close to the interfaces with $\theta_{N,n} \approx 0$ and $Q_{N,n} \approx (2\pi/a)(1 \pm n/(N-1))$, where n is the number of SDW nodes in the spacer. More surprisingly, the authors found that for $N > 40$ an I SDW with two nodes is distorted by the admixture of a C SDW. Niklasson *et al* also verified that in the presence of a SDW, the DOS of the trilayer is partially gapped near the Fermi level.

Even within this group of first-principles calculations, there is great disagreement about the magnitude of the exchange coupling. For example, the IEC obtained by Mirbt *et al* [73] is about seven times larger than that predicted by Hirai [19]. It is possible that the thinness of the Fe layers (only 3 or 4 ML) lowers the exchange coupling within the latter calculation.

3.2. Experiments on Fe/Cr wedges and trilayers

Due to poor sample quality, the first measurements of the IEC and GMR [10] revealed only a long-period oscillation. After the short-period oscillation was discovered in Fe/Cr wedges [4, 5], a huge effort was devoted to measurements of the exchange coupling, some of which are discussed below.

3.2.1. SEMPA measurements. The basic geometry of the NIST measurements [4, 21] is displayed in figure 8, where a Cr wedge is built atop an Fe (100) whisker with two halves magnetized in opposite directions. A thin Fe film of 20 Å overlays the Cr wedge. SEMPA measurements were used to image the magnetization of the top layers of the Cr wedge and Fe overlayer. Comparison of figures 9(c) and 9(d) reveals that the Fe overlayer is AF coupled to the Cr layer below. For $N \leqslant 3$, the Fe moments on either side of the Cr wedge were F coupled; then up to $N = 11$, they were AF coupled. Similar results had previously been reported based on BLS measurements [74]. But for $N > 11$, Unguris *et al* [21] found an alternating, 2 ML coupling which repeats every 20 ML at room temperature, as shown by figures 9(b) and 9(c). Since the Néel temperature of the thin Cr spacer was expected to be lower than $T_N^{bulk} \approx 311$ K [75], the authors conjectured that a SDW must be stabilized by the Fe–Cr interfacial coupling.

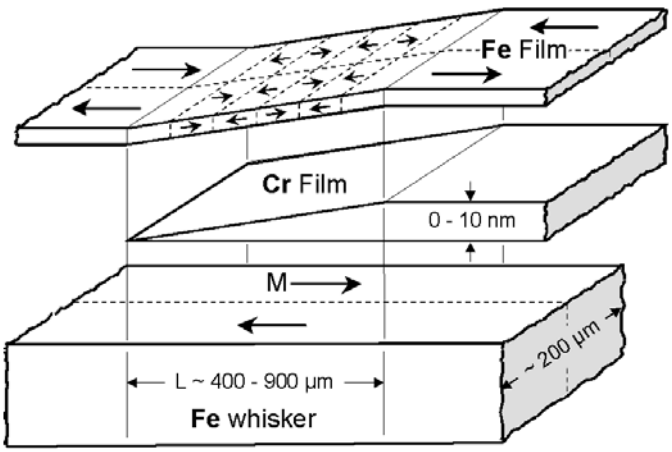

Figure 8. The geometry of the Fe/Cr wedge used in the NIST measurements [4].

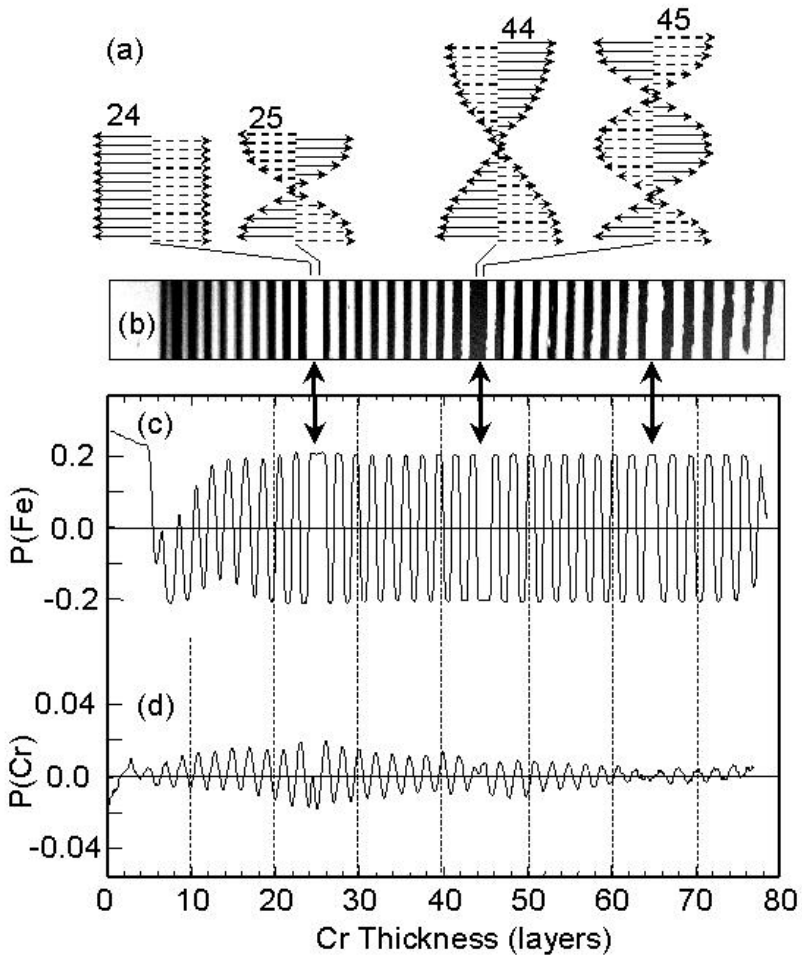

Figure 9. (a) The conjectured SDWs for thicknesses on either side of two phase slips. (b) A SEMPA image of the magnetization of the Fe film covering the wedge, with arrows marking the Cr thickness where phase slips are found. (c) Spin polarization of the Fe overlayer. (d) Spin polarization of the topmost Cr layer before depositing the Fe overlayer [77].

Remarkably, the temperature dependence of the phase-slip distance plotted in figure 10(a) was found to be quite similar to that of the distance between SDW nodes in bulk Cr. As speculated by Unguris *et al* and demonstrated in section 2, the separation between SDW nodes in the Cr spacer may be significantly reduced by the 0.6% lattice mismatch between Fe and Cr. Assuming that the phase-slip distance is equivalent to the distance between SDW nodes, figure 10(a) implies that the I SDW period increases with temperature and may diverge at about 650 K, above which the SDW would become commensurate. The SEMPA measurements were stopped at 550 K to avoid damaging the sample. But even if measurements were available up to much higher temperatures, it would still be impossible to prove that the SDW had become commensurate: all that can be determined is that the node-to-node distance $a/2\delta'$ exceeds the length of the wedge.

Replotted in figure 10(b), the NIST measurements [76] can be compared with the phenomenological phase diagram of figure 4(b) [45]. According to the phenomenological model, the SDW is commensurate prior to the first phase slip, has $n = 1$ node between the first and second

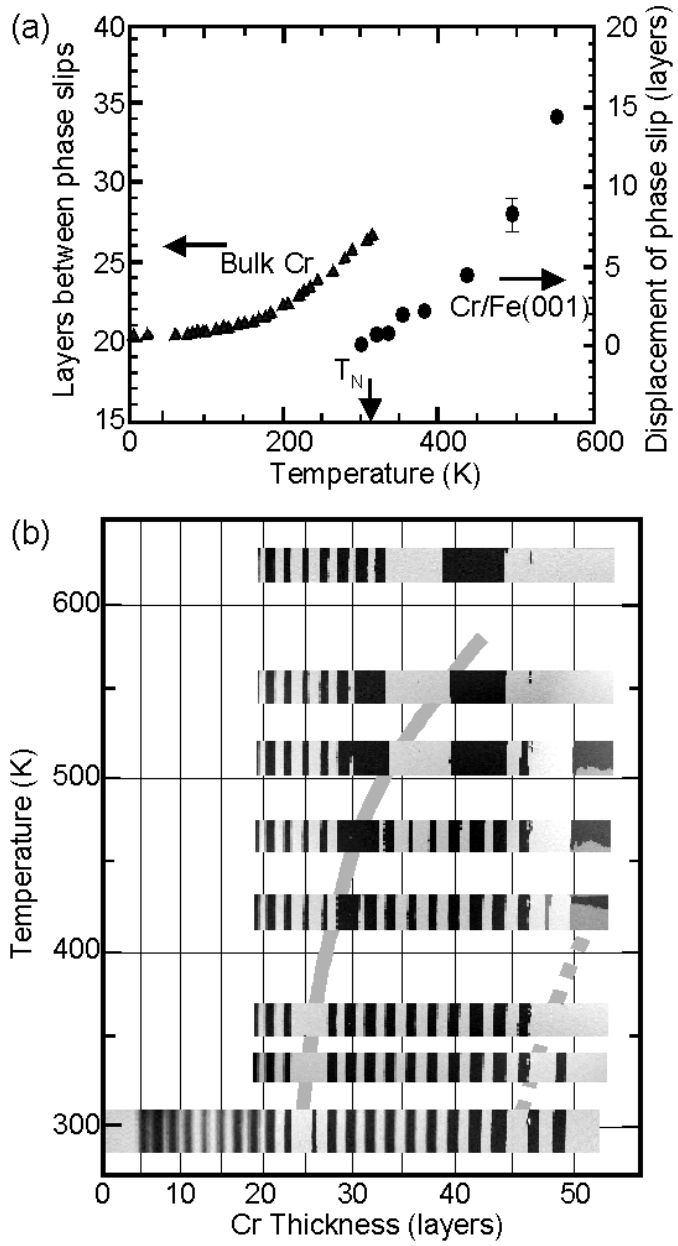

Figure 10. (a) The temperature dependence of the node-to-node distance in bulk Cr and the distance between phase slips in an Fe/Cr wedge. The bulk Néel temperature is marked by an arrow. (b) The temperature dependence of the IEC in an Fe/Cr wedge with the solid curve denoting the first phase slip in a bare wedge and the dashed curve providing an estimate of the second phase slip [77].

phase slips, and $n = 2$ nodes to the right of the second phase slip. Some of the conjectured SDW configurations are pictured in figure 9(a) [77].

Because the short-period coupling decays more rapidly with temperature than the long-period coupling [76], measurements of the bare Cr wedge were used in figure 10(b) to determine

the positions of the phase slips at elevated temperatures. Measurements of thin Cr films grown on Fe [78, 79] reveal that the surface moment of Cr is substantially enhanced from its bulk value. This suggests that SDW antinodes tend to lie at a free Cr surface. Such behaviour is corroborated by figure 9(d), where the polarization of the topmost layer of the Cr wedge is squared up for $N > 24$. Since both the Fe–Cr and vacuum–Cr interactions act to place the SDW antinode at the interface, some predictions made for an Fe/Cr/Fe wedge may also be relevant to the bare Fe/Cr wedge. Nevertheless, this argument does not explain why the phase slips are unshifted by the different strengths of the Fe–Cr and vacuum–Cr interactions.

Unlike most other properties, the sign of the IEC cannot be explained by a model for a perfect trilayer. Prior to the first phase slip, such models predict that the magnetic coupling is F for odd N and AF for even N. In fact, the opposite behaviour was observed at NIST. As discussed in the next section, this sign reversal is probably caused by Fe–Cr interdiffusion.

3.2.2. Measurements of the BL coupling. Although the SEMPA measurements were revelatory, they could not be used to determine the magnitude of the exchange coupling. A trilayer with angle ϕ between Fe moments on either side of the Cr spacer is often described by the bilinear–biquadratic (BL–BQ) model with energy

$$E = -J_1 \cos(\phi) + J_2 \cos^2(\phi) \tag{7}$$

where J_1 and J_2 are the BL and BQ couplings, respectively. It follows that $J_c = E_{AF} - E_F = 2J_1$ is independent of J_2. Also note that CF conditions correspond to $\phi = 0$ (odd N) or π (even N). If J_1 is small and $J_2 > 0$, then the equilibrium value for ϕ is close to $\pi/2$.

The two most powerful techniques for measuring J_1 and J_2 are MOKE and BLS measurements, often used in tandem. Indeed, BLS was employed by Grünberg *et al* [1, 74] in the original discovery of AF coupling between the Fe moments for $4 < N < 10$. Both MOKE and BLS measurements can be used to obtain J_1 and J_2 in AF-coupled samples from the critical fields H_1 and H_2. Below H_1, the Fe moments remain antiparallel with $\phi = \pi$; between H_1 and H_2, ϕ lies between π and 0; for $H > H_2$, the Fe moments are parallel with $\phi = 0$. In a F-coupled sample, there is a single constraint on J_1 and J_2 and BLS measurements can only [80] be used to determine the total exchange coupling $J_1 + 2J_2$.

Assuming that J_2 is the same for F-coupled samples as for AF-coupled samples with one less ML of Cr, Heinrich *et al* [81, 82] obtained the coupling strengths plotted in figure 11. Notice that the short-period, 2 ML oscillation exhibits the same delayed onset as in the SEMPA measurements but can be distinguished even in the regime with an AF bias. Like SEMPA measurements, BLS measurements also indicate that J_1 has the opposite sign compared to the predictions for a perfect trilayer. The magnitude $J_1 \sim 1$ erg cm^{-2} obtained by the Simon Frazer group [82] is just a bit smaller than that found by Barthélémy *et al* [6] from the saturation magnetization and only slightly larger than the BLS results reported by Grünberg *et al* [74]. We shall forgo a discussion of the magnitude and significance of J_2 until section 4.

3.3. Conditions for non-collinear SDWs in perfect trilayers

The development of non-collinear moments in a superlattice composed of alternating F and AF materials was first considered theoretically by Hinchey and Mills [83] based on a Heisenberg model. For even N, they argued that applying a magnetic field to align the F layers would create a 'superlattice spin-flop phase' in which the moments of the AF layers form a non-collinear structure.

Stoeffler and Gautier [84] conjectured that a non-collinear SDW could be stabilized in an Fe/Cr trilayer under non-CF conditions. As shown in figure 12, the SDW may preserve the

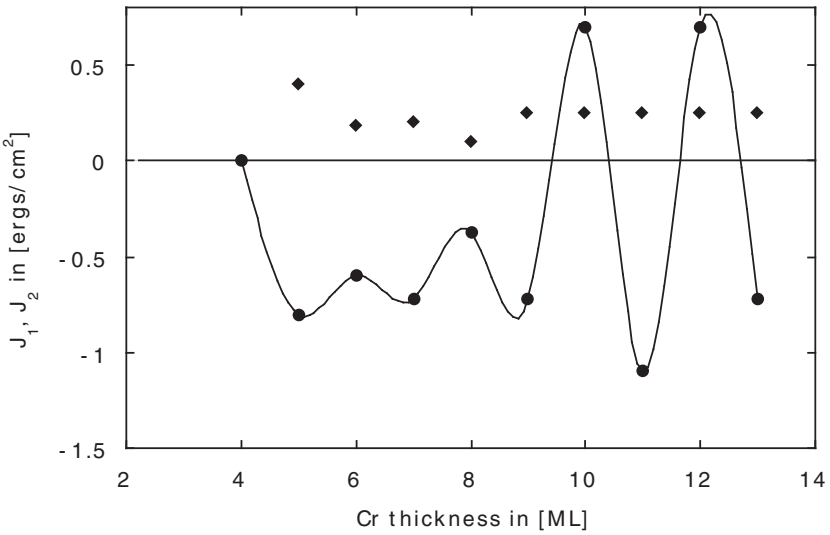

Figure 11. The thickness dependence of J_1 (circles) and J_2 (diamonds) from BLS and MOKE measurements [82].

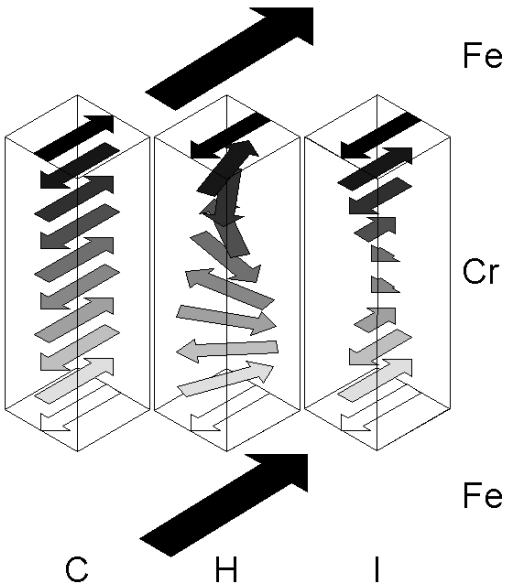

Figure 12. Three possible SDW states when the Fe moments are non-CF [88].

interfacial energy by forming either an I SDW with a single node or a H SDW with a π-twist. For large N, the H SDW only costs a small amount of energy compared to a C SDW. So if a bulk I SDW with $1/\delta' = N$ has a sufficiently high free energy compared to a bulk C SDW, the H SDW would have the lowest free energy in the trilayer.

Informed by a d-band tight-binding calculation, Stoeffler and Gautier [84] concluded that the H SDW is favoured over a collinear I SDW under non-CF conditions when $N \geqslant 24$. However, a different non-collinear state which has a larger twist at the centre of the spacer but is more nearly collinear at the interfaces was found to have lower energy than either the H or I SDWs for $N \geqslant 20$. Presumably, these calculations were performed using material parameters

that favour C over I SDWs in bulk Cr with the result that the non-collinear SDW approaches a C SDW in the limit of large N or small twist. Stoeffler and Gautier argued that an I SDW is preferred at low N due to the suppression of the H SDW moments when its period a/δ' is too small. According to their calculations, the H SDW disappears when the angle $\pi(1-\delta')$ between moments on neighbouring ML is less than 0.95π or when δ' exceeds 0.05. So for $N < 20$ and non-CF Fe moments, a H SDW is prohibited and an I SDW is stable. But this simple argument ignores the similar suppression of the I SDW moments when δ' exceeds its bulk value. Later tight-binding calculations by Freyss *et al* [85] found that the torque created by a non-collinear SDW also induces some degree of non-collinearity within the Fe layers themselves.

To bolster their case for the stability of a non-collinear SDW, Stoeffler and Gautier [86] also studied the l–J model with energy

$$E(\{\boldsymbol{M}_i\}) = \sum_i l(\boldsymbol{M}_i) + J \sum_{\langle i,j \rangle} \boldsymbol{M}_i \cdot \boldsymbol{M}_j \tag{8}$$

where

$$l(\boldsymbol{M}_i) = A\boldsymbol{M}_i^2/2 + B\boldsymbol{M}_i^4/4$$

is the 'formation' energy for the moments. All of the atoms in the ith ML are assumed to have the same moment $\boldsymbol{M}_i$, so the sums run from $i = 1$ to N. By fitting this local-moment model to the predictions of the tight-binding model, the authors estimated that $A = 608$ meV/atom, $B = 28$ meV/atom, and $J = 309$ meV/atom. Since exchange coupling is sacrificed by the nodes of an I SDW, the l–J model favours C over I ordering. Taking $\boldsymbol{M}_1$ and $\boldsymbol{M}_N$ to be parallel for even N and antiparallel for odd N (the non-CF conditions), Stoeffler and Gautier obtained the minimum energies plotted in figure 13, where the collinear state is an I SDW. Although not helical, the minimum-energy configuration for $N \geqslant 20$ is non-collinear and approaches the H state as $N \to \infty$. If the competition is restricted to I and H phases, then the H SDW becomes stable for $N \geqslant 27$.

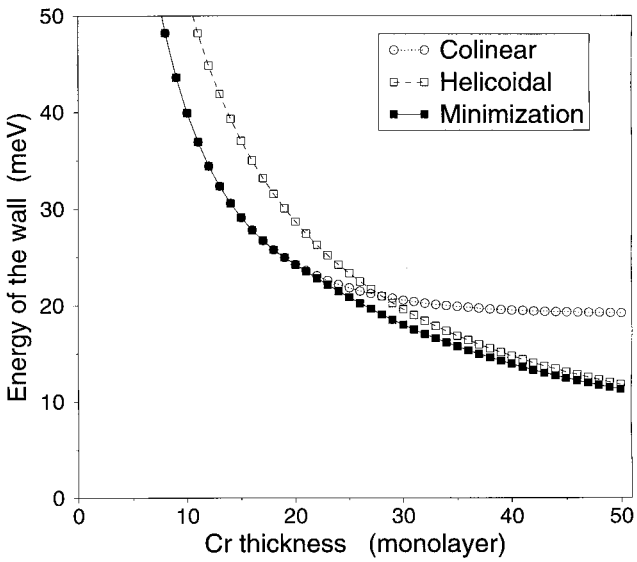

Figure 13. The energy per atom in meV of collinear I (open circles), H (filled squares), and non-collinear (filled squares) states constrained by the condition that $\boldsymbol{M}_1$ and $\boldsymbol{M}_N$ satisfy non-CF conditions [86].

However, recent tight-binding calculations by Cornea and Stoeffler [87], which include s and p as well as d contributions to the electronic density and use improved tight-binding parameters appropriate for pure Cr, now indicate that the central moments in a non-collinear SDW are suppressed as ϕ deviates from CF conditions. By the point at which non-CF conditions are reached, the central moments have deformed into a node and the SDW has become incommensurate and collinear. Thus, for an AF-coupled trilayer, a non-collinear SDW is stable between the critical fields H_1 and H_2 but disappears above H_2.

The phenomenology introduced above was generalized by Fishman [88] to study the competition between H and I SDWs in a perfect trilayer with non-CF Fe moments. Along the IH phase boundary $T_{\rm IH}(z_0)$ for large N, both SDWs have a period of $a/\delta' = 2(N-1)$. That is to say, the I SDW contains a single node and the H SDW undergoes a single π-twist in the Cr spacer. Above $T_{\rm N}^{\rm bulk}(z_0)$, $T_{\rm IH}(z_0)$ was found to be independent of the coupling constant γ and to increase with the energy mismatch z_0. Below $T_{\rm N}^{\rm bulk}(z_0)$, $T_{\rm IH}(z_0)$ lies to the left (smaller z_0) of the bulk CI phase boundary $T_{\rm IC}(z_0)$. So the stability of the bulk C phase does not imply that the H phase will be stable in a perfect trilayer with non-CF moments. Rather, the bulk C phase must be sufficiently lower in free energy than the bulk I phase for the H phase to be stable in the trilayer; otherwise the I phase will have the lowest free energy.

4. SDWs in trilayers and multilayers with interfacial disorder

As evident from the sensitivity of the short-period coupling to sample quality, interfacial disorder has a dramatic effect on the properties of an Fe/Cr trilayer. Two kinds of disorder are discussed in this section. First we consider the relatively benign effects of Fe–Cr interdiffusion, in which some interfacial Fe and Cr atoms are switched. Then we consider the more severe consequences of interfacial steps. This section ends with a discussion of the BQ coupling in trilayers and multilayers.

4.1. Fe–Cr interdiffusion

Early experimental studies of Fe–Cr interdiffusion were primarily motivated by the sensitivity of the short-period coupling to sample quality [9,89]. But the delay in the onset of this coupling and its sign reversal [4,5] also required explanation. Several early studies [9,21,89,90] revealed that interfacial quality can be somewhat controlled by regulating the substrate temperature during growth. Later studies [91–93] specifically addressed the effect of sample preparation on Fe–Cr interdiffusion. Davies *et al* [93] noticed that upon initial deposition, only one in four Cr atoms remains in the surface layer, the rest substituting for Fe atoms in the interfacial Fe layers. Only above 1 ML coverage does the surface consist primarily of Cr atoms. Because Fe has a lower melting temperature than Cr, interdiffusion is restricted to the bottom of the Cr wedge and is not observed near the Fe overlayer [92]. In fact, the sign of the coupling can be reversed by intentionally depositing [94] a mixed Cr–Fe layer below the Fe overlayer. Whereas both forms of interfacial disorder suppress the short-period coupling, Fe–Cr interdiffusion has a particularly large impact on the GMR [95].

Tight-binding models have been very successful at treating the effects of Fe–Cr interdiffusion. If one quarter of the Fe and Cr atoms are switched within 2 ML of each interface, then the exchange coupling is deeply depressed and the short-period oscillations are washed out [17], as shown in the dashed curve of figure 6. The interdiffused interface also suppresses the nearby Cr moments. Assuming that interdiffusion is restricted to a single interface as in an Fe/Cr wedge, Freyss *et al* [85] found that interchanging more than one quarter of the Cr and Fe atoms in the first 2 ML reverses the sign of the exchange coupling. This has recently

been verified by first-principles calculations [96]. For comparison, three quarters of the Cr and Fe atoms are interchanged within 2 ML of the Fe whisker in the sample studied by Davies *et al* [93].

4.2. Interfacial steps

In contrast to the benign effects of Fe–Cr interdiffusion, interfacial steps have severe consequences. As shown in figure 14 for a C SDW in the Cr spacer, the Fe and Cr moments can respond to the frustration of a step in at least three ways. In figure 14(b), the frustration remains at the Fe–Cr interface and the C SDW is decoupled from the Fe layer. To maintain the coupling energy, domains may form in either the Fe or Cr layers, as pictured in figures 14(c) and 14(d).

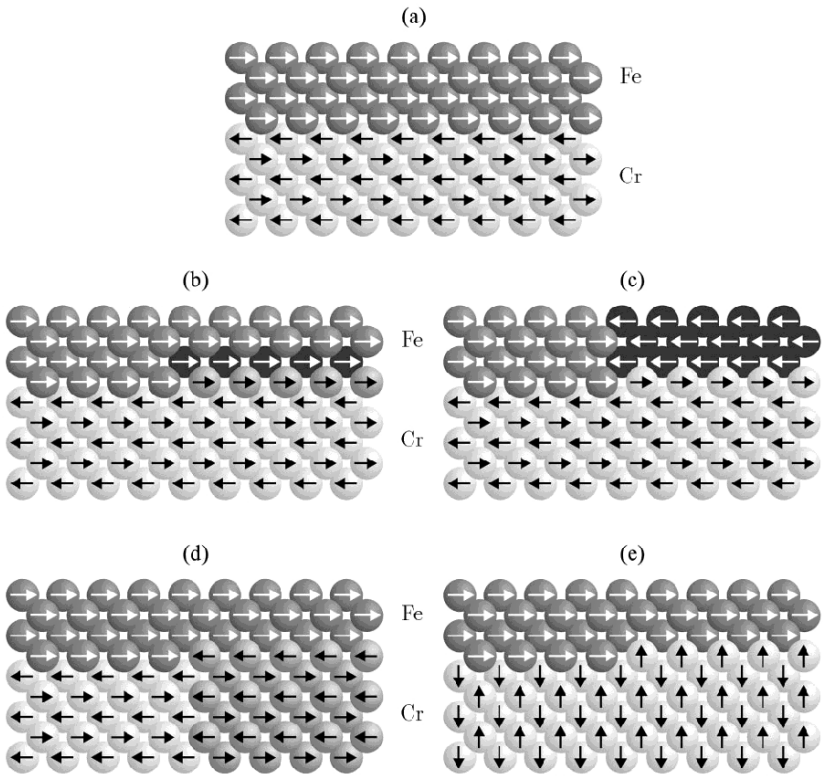

Figure 14. Schematic representation of the interaction between a thin Fe film and a C SDW in a Cr spacer, with white arrows representing the moments in the Fe and black arrows the moments in the Cr [101]. Starting with (a) a perfect interface with AF coupling between the Fe and Cr, there are four ways of responding to an interfacial step: (b) frustration at the interface, (c) domains in the Fe layer, (d) domains in the Cr spacer, and (e) reorientation of the SDW.

It is difficult to treat interfacial disorder within RKKY and quantum-well models because interfacial steps destroy the in-plane translational invariance of the free energy. Therefore, the parallel component of the electron momentum is no longer a good quantum number and a single momentum state can be scattered into several nearby states [59]. Formally, surface roughness can be characterized as correlated (repeated from layer to layer) or random [97], which may be distinguished in x-ray measurements.

4.2.1. Theoretical SDW response to a rough interface. Besides forming C or I domains, a SDW may respond to the presence of an interfacial step in several ways. In analogy with equation (6), the direct Fe–Cr coupling energy at an interface can be written as

$$E_i = \frac{1}{2} J_i \boldsymbol{S}_{\rm Fe} \cdot \left\{ \boldsymbol{S}_{\rm Cr}(a/2) + \boldsymbol{S}_{\rm Cr}(a) \right\}. \tag{9}$$

For a C SDW, E_i always vanishes. But for a T SDW with $\boldsymbol{Q}'_{\pm}$ out-of-plane and moments in-plane, E_i becomes

$$E_i = -J_i \boldsymbol{S}_{\rm Fe} \cdot \hat{\boldsymbol{m}} \alpha_s g \sin(\pi\delta'/2) \sin(3\pi\delta'/2 + \theta) \tag{10}$$

which is minimized when $\hat{\boldsymbol{m}}$ is parallel to $\boldsymbol{S}_{\rm Fe}$ and $\theta = \pi/2 - 3\pi\delta'/2$. This implies that $E_i = -J_i S_{\rm Fe} S_{\rm Cr}(a/2)$ where $\boldsymbol{S}_{\rm Cr}(a/2) = \boldsymbol{S}_{\rm Cr}(a) = -\hat{\boldsymbol{m}} \alpha_s g \sin(\pi\delta'/2)$, corresponding to a node of the T SDW lying between planes $z = a/2$ and $z = a$. Since $\pi\delta'/2 \approx \pi/40$, E_i is about 13 times smaller than for a T SDW antinode at a perfect interface.

Assuming that I SDW nodes lie at both interfaces, Fishman [46, 98] used a phenomenological model to construct the magnetic phase diagram. Since at least a half-period of the SDW must occupy the spacer, the Néel temperature $T_{\rm N}^{\rm lay}$ of the trilayer vanishes when the thickness is less than about 20 ML. With increasing thickness, the SDW first stretches and then contracts with the introduction of another node. Whenever the node-to-node distance $1/\delta' = (N-1)/n$ passes close to its bulk value, $T_{\rm N}^{\rm lay}$ reaches a maximum. As a result, $T_{\rm N}^{\rm lay}(L)$ exhibits a seesaw pattern, with minima at the transitions between SDW states with different numbers $n + 1 \geqslant 2$ of nodes.

The proximity magnetism or torsion model developed by Slonczewski [99] calls for two domains of H SDWs with opposite helicities that couple the Fe moments non-collinearly, as shown in figure 15. If the domains with thickness N are larger than those with thickness $N \pm 1$, then the angle ϕ between the Fe moments may differ from 90 degrees. Slonczewski originally suggested that the Cr moments are induced by their proximity to the Fe layers and that the Cr spacer favours collinear ordering. That bulk Cr actually has an innate tendency towards H ordering with a period of $a/\delta' \approx 30a$ strengthens some aspects of this model but weakens others. More details about the torsion model will be provided shortly.

Fishman [100] constructed a phenomenological free energy like the one in equation (6) for the competition between I and H SDWs in the presence of interfacial steps. As shown in figure 16, pairs of H SDWs with twists $\pm|m|\pi/2$ (m odd) have a lower free energy than an I SDW for small thickness or high temperature. The total twist of each H SDW increases with N, so the SDW period remains close to its bulk value of about 60 ML (corresponding to a twist of 2π). This result differs from the torsion model, which requires that $m = \pm 1$ for any thickness. Below the solid curve, the I SDW nodes remain close to the interfaces, in accord with the coupling energy E_i introduced above, and the I SDW wavevector changes discontinuously across the solid vertical lines. If the H SDW is restricted to a single twist of $\pm\pi/2$ (as in the torsion model), then the H and I phases would be separated by the dashed phase boundary.

The weak magnetic field produced by the Fe layers acts on a greater number of Cr moments further away from the interface than the Fe–Cr exchange coupling. In a thick Cr spacer, this field may overcome the direct interfacial interaction by reorienting the SDW moments. Because $\chi^{\perp} > \chi^{\parallel}$, the energy of a SDW is lowest when its moments are perpendicular to the Fe moments. For a T SDW, the ordering wavevectors $\boldsymbol{Q}'_{\pm}$ will point along the field direction, parallel to the Fe moments, and the spins may lie either in-plane or out-of-plane (in either case being perpendicular to the Fe moments). For a L SDW, the SDW wavevectors and moments (which are parallel) may lie either in-plane and perpendicular to the Fe moments or out-of-plane.

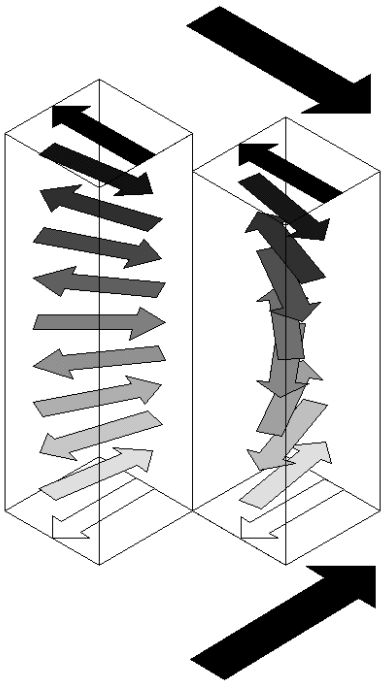

Figure 15. A sketch of two H SDWs, one right handed and the other left handed, coupling Fe moments at a 90° angle due to a step at the interface [100].

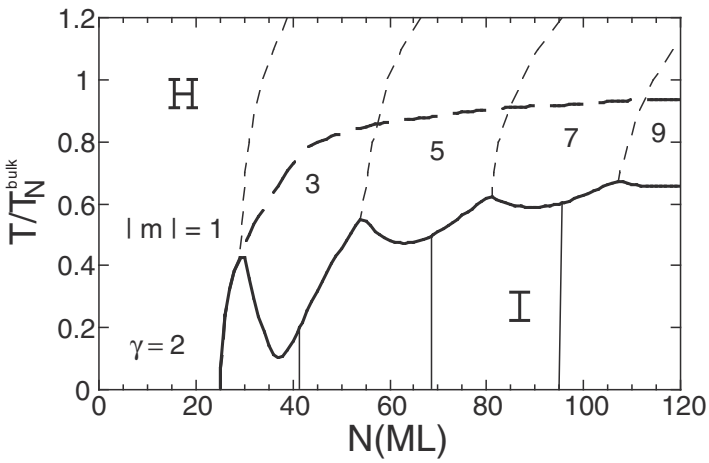

Figure 16. The phase diagram of an Fe/Cr trilayer containing interfacial steps, using $\gamma = 2$ and $z_0/T_N^* = 5$ [100]. The thick solid curve gives the temperature of the transition between an I SDW and a H SDW with a twist of $m\pi/2$. The thick dashed curve gives the phase boundary between an I SDW and a H SDW with a single twist of $\pm\pi/2$.

For small spacers, SDW domains may form in the Cr spacer as in figure 14(d). Following the argument of Bödeker *et al* [101], domains appear when the energy lost at the domain walls is less than the energy lost by frustration at the Fe–Cr interface or when $L < J_{\mathrm{Fe-Cr}} L_s / J_{\mathrm{Cr-Cr}}$, where L_s is the distance between steps and $J_{\mathrm{Fe-Cr}} = J_i S_{\mathrm{Fe}} S_{\mathrm{Cr}}$ and $J_{\mathrm{Cr-Cr}}$ are the effective

exchange energies for spins of *unit length* at $T = 0$. This estimate corresponds to a thickness of roughly 250 Å, which is consistent with the measurements discussed below. Bödeker *et al* [48] also studied the reorientation of the Cr moments in thick spacers guided by simulations of the classical Heisenberg model, obtaining the spin configuration schematically represented in figure 14(e) with moments out-of-plane.

4.2.2. Observed SDWs in multilayers and films. Although it is the sole sure-fire technique for detecting SDWs, neutron scattering is only useful for studying Cr films or Fe/Cr superlattices with total Cr thicknesses greater than a few hundred ängströms. Because Fe/Cr superlattices cannot be grown with the same precision as Fe/Cr wedges, they contain rougher interfaces with shorter terrace lengths L_s. Despite a preliminary report in 1990 [6], the first confirmed measurements of SDWs in an epitaxially grown Fe/Cr multilayer [23, 24] came five years later. Subsequent neutron-scattering measurements [25, 26] on sputtered multilayers followed quickly. Both sets of measurements agree on a few points: at low temperatures, an I SDW only appears above a critical thickness of about 30 ML; at large thickness, it only appears below a critical temperature of about 300 K. In the phase space occupied by the I SDW, the coupling between the Fe moments is too weak to detect; outside this region, a strong BQ coupling was observed.

But where measurements on sputtered multilayers [25] detected only weak scattering below 30 ML and above 300 K, measurements on epitaxially grown multilayers [24] revealed a H SDW in the phase space not occupied by an I SDW up to at least 500 K, as shown in figure 17. By 'C' order, Schreyer *et al* [24] meant the H modulation of the SDW with the same moment on every site. They also observed a transition region 'T' where I and H SDWs coexist. Comparing figures 16 and 17, it seems likely that higher-order H SDWs with three or more twists of $\pm\pi/2$ coexist with an I SDW in the 'T' region while H SDWs with a single twist of $\pm\pi/2$ are restricted to the 'C' region. According to the arguments in reference [100], higher-order H SDWs may be more easily destroyed by magnetic impurities than an I SDW, which can place its nodes at the impurity sites. As recently demonstrated by MOKE measurements [102], the Néel temperature $T_{\mathrm{N}}^{\mathrm{lay}}$ of an epitaxially grown multilayer increases from about 500 K at $L = 55$ Å to 600 K at 15 Å, with the Fe moments decoupled above $T_{\mathrm{N}}^{\mathrm{lay}}$. The increase of $T_{\mathrm{N}}^{\mathrm{lay}}(L)$ with decreasing L was attributed to the greater effectiveness of the Fe–Cr interfacial interactions at stabilizing a SDW in a small spacer.

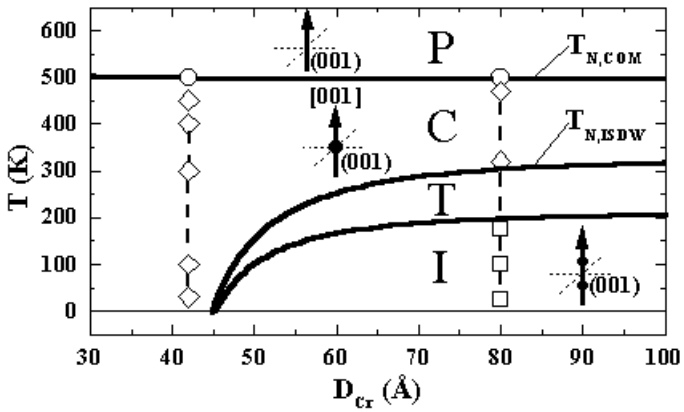

Figure 17. The phase diagram of an Fe/Cr multilayer reporting I, 'C' (really H), and P phases, as well as a transition region 'T' where I and H SDWs coexist [24].

Fourier analysis of the neutron-scattering measurements taken by Fullerton *et al* [25] on sputtered multilayers yielded the SDW configurations in figure 18, with the SDW nodes lying at the Fe–Cr interfaces for the two thicker spacers. No significant H or C signal was reported and the Néel temperature of the multilayer vanishes [103] below a critical thickness of about 30 ML. Although similar behaviour follows from a model which forces the SDW nodes to lie at the interface, the measured Néel temperature $T_N^{lay}(L)$ is a monotonic function of thickness with none of the dips or peaks predicted by reference [98]. In fact, the measured $T_N^{lay}(L)$ lies very close to the phase boundary between the 'T' and 'C' regions in figure 17. As discussed above, the exchange coupling E_i mediated by an I SDW at a rough interface is far smaller than in the absence of interfacial steps and may be undetectable in neutron-scattering measurements.

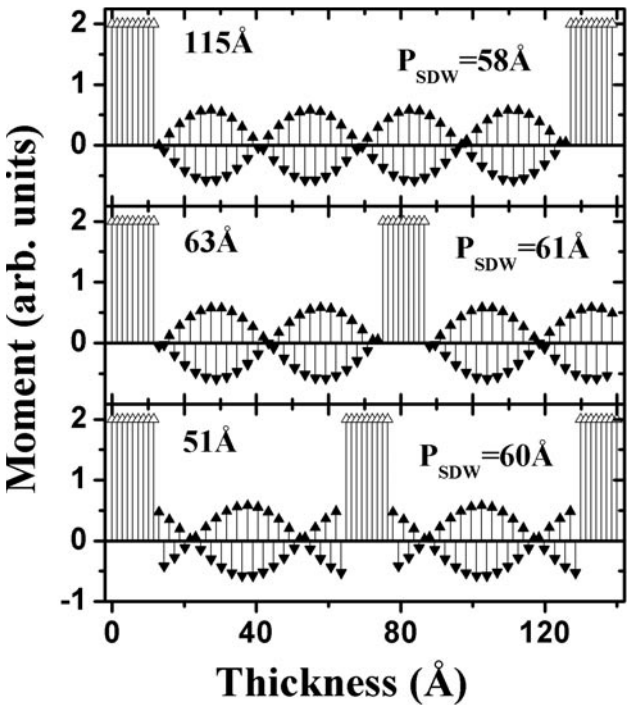

Figure 18. Spin configurations based on neutron-scattering results for Fe/Cr multilayers for three values of the Cr thickness [25]. Filled and open arrows represent the Fe and Cr moments, respectively. The period of the SDW is also indicated for each sample.

The disagreements between Schreyer *et al* and Fullerton *et al* are probably caused by the different methods used to fabricate their samples. It is believed that the sputtered multilayers at Argonne are rougher than the epitaxially grown multilayers at Bochum. In sputtered multilayers, the SDW order parameter may be suppressed within ξ_0 of the interface, thereby preventing the development of nodeless, C or H SDWs. By comparison, the wider terraces of the epitaxially grown multilayers may permit the formation of H domains. According to Bödeker *et al* [101], the minimum terrace length to allow SDW domains is $L_{s,\min} = J_{Cr-Cr}L/J_{Fe-Cr} \approx 0.25L$.

In contrast to the multilayer measurements described above, Meersschaut *et al* [104] found that the SDW in Fe/Cr multilayers is longitudinal with moments out-of-plane for 75 Å $< L <$ 400 Å. At low temperatures, perturbed angular correlation spectroscopy (PACS) measurements indicated that the SDW disappears below about 60 Å or 40 ML. For bulk Cr [105]

and thin Cr films [106], strain can produce a L SDW with $\boldsymbol{Q}'_{\pm}$ normal to the surface. PACS measurements on Ag/Cr multilayers [107] suggest that the observed L SDW with wavevectors and moments out-of-plane is also produced by strain.

Thus far, we have not pondered the fate of the spin-flip transition observed in bulk Cr at $T_{\mathrm{SF}} = 123$ K. In the Fe/Cr multilayers studied by the Bochum and Argonne groups, it seems likely that $T_{\mathrm{SF}} = 0$, so a L SDW is never stable. In Fe/Cr bilayers, however, a L SDW with moments in-plane but perpendicular to the Fe moments [108] produces a large coercive field below 130 K [109]. The reduction of the remanent magnetization above 130 K is attributed to a T SDW coupled to Fe domains as in figure 14(c). Recent magnetization measurements [108] indicate that T_{SF} decreases with decreasing film thickness.

We shall not spend much more time discussing Fe/Cr bilayers except to note that virtually every possible SDW with moments perpendicular to the Fe moments has been observed [28, 48, 101] for $L > 250$ Å. As mentioned above, this spin reorientation may be attributed to the different parallel and perpendicular susceptibilities of bulk Cr.

Finally, there is the related question of how the Néel temperature $T_{\mathrm{N}}^{\mathrm{film}}(L)$ of a thin Cr film depends on thickness in the absence of adjoining Fe layers. Due to the contribution of the surface free energy, scaling theory predicts that $T_{\mathrm{N}}^{\mathrm{film}}(L)$ is suppressed with decreasing L [103]. However, both Mattson *et al* [75] and Sonntag *et al* [106] concluded that strain energies dominate this 'finite-size' effect. While $T_{\mathrm{N}}^{\mathrm{film}}(L)$ increases with L for Cr on a LiF substrate [75], $T_{\mathrm{N}}^{\mathrm{film}}(L)$ decreases with L for Cr on a Nb film on a sapphire substrate [106].

4.3. BQ coupling

One of the most important discoveries in Fe/Cr trilayers and multilayers was the dominance of the BQ coupling between the Fe moments for certain ranges of thickness and temperature. Although first observed almost ten years ago [110], the origin of the BQ coupling in Fe/Cr trilayers and multilayers is still being debated. This subsection will first discuss models of the BQ coupling, then review measurements of J_2, and finally examine the possible role of non-collinear SDWs.

4.3.1. Models of the BQ coupling. We shall introduce four models for the BQ coupling. While the two intrinsic models do not require disorder, the two extrinsic models assume interfacial steps.

Several groups [111–113] have proposed intrinsic models for the BQ coupling based on a quantum-well approach. In every case, the predicted value for J_2 is much too small to explain the experimental observations. For example, Erickson *et al* [111] concluded that the maximum J_2 is about 1% of the maximum J_1. This is roughly 15 times too small [110]. Another flaw of such models is that the predicted J_2 oscillates about 0 while the observed J_2 is always positive.

Slonczewski [99, 114] realized that changes in the BL coupling due to thickness variations will produce a BQ coupling. If J_1 alternates between F and AF, then the Fe moments on either side of the spacer will respond to the fluctuation ΔJ_1 by aligning at an average angle of 90 degrees. The predicted coupling constant

$$J_2 \propto L_s \frac{(\Delta J_1)^2}{A} \tag{11}$$

is inversely proportional to the exchange stiffness A in the Fe layer and increases with L_s until J_2 equals ΔJ_1, at which point the thickness-fluctuation model breaks down.

Also developed by Slonczewski [99], the torsion model was introduced in figure 15, where two domains of H SDWs in spacers of thickness N and $N \pm 1$ couple the Fe moments at a

90° angle. Slonczewski assumed that the SDW in a domain of thickness N prefers a C SDW with $\phi = 0$ (odd N) or π (even N) and that the angle of deviation of the Cr spin axis from one layer to another is small. Thus, the coupling energy is either $C_+\{\phi\}^2$ or $C_-\{\phi - \pi\}^2$, where $C_\pm \sim 1/N$. The brackets restrict the angles to lying between $-\pi$ and π, so the H SDW cannot twist around by more than $\pm\pi$. Adding the coupling energies of the two domains yields

$$E = C_+\{\phi\}^2 + C_-\{\phi - \pi\}^2 \tag{12}$$

which should then be used in place of equation (7). For a single domain with even or odd N, C_+ or C_- vanishes. If the domains of size N and $N \pm 1$ are equally populated, then $C_+ = C_-$ and the equilibrium angle between the Fe moments is $\phi = \pi/2$. To guarantee that the Fe moments are uniform within each layer, the torsion model requires that $L_s < 100$ Å.

Using a d-band tight-binding model, Freyss *et al* [115, 116] tried to justify the torsion model. For a single domain of thickness $N \geqslant 5$, the energy was found to be nearly quadratic in $\Delta\phi = \phi$ (odd N) or $\pi - \phi$ (even N) and so to fit the form of equation (12). Although the Cr moments at the centre of the spacer contract as $\Delta\phi$ increases, the SDW remains non-collinear even when non-CF conditions are achieved with $\Delta\phi = \pi$. But the recent tight-binding calculations of Cornea and Stoeffler [87] indicate that the SDW becomes incommensurate and collinear as $\Delta\phi$ approaches π. Due to the flattening of the energy near $\Delta\phi = \pi$, the BL–BQ model provided a better fit to their results.

Magnetization measurements can be used to distinguish the torsion and BL–BQ models. Unlike the latter, the former yields a non-vanishing torque $\mathrm{d}E/\mathrm{d}\phi$ when $\phi = 0$. So within the BL–BQ model, the saturation magnetization with $\boldsymbol{S}^{\mathrm{I}}_{\mathrm{Fe}} = \boldsymbol{S}^{\mathrm{II}}_{\mathrm{Fe}}$ or $\phi = 0$ can be achieved at a finite field. But the torsion model implies that a non-zero torque is always exerted on the Fe moments, so saturation can only be approached asymptotically.

Stoeffler and Gautier [86] proposed another intrinsic model for the BQ coupling based on the l–J model introduced in equation (8). For $\Delta\phi$ near $\pi/2$, the SDW is predicted to be non-collinear with greatest twist at the centre of the spacer. This non-collinearity produces a BQ term with $J_2 \approx 0.15|J_1|$ for $N = 9$ or 10. Unfortunately, few other details were provided about this model and several questions remain. For example, is the BL–BQ form still valid for $N \geqslant 20$, in which case the l–J model predicts (see figure 13) that the SDW remains non-collinear when $\Delta\phi = \pi$? Within the recent tight-binding calculations of Cornea and Stoeffler [87], the non-collinearity of the SDW for $0 < \Delta\phi < \pi$ and $N \geqslant 10$ is also responsible for an intrinsic BQ coupling $J_2 \approx |J_1|/3$. But in either model, the predicted value of J_2/J_1 is too small to stabilize a non-collinear coupling between the Fe moments in zero field. So to explain the experimental measurements described below, these intrinsic mechanisms must be combined with an additional extrinsic contribution to J_2.

4.3.2. Measurements of the BQ coupling. The BL–BQ model of equation (7) predicts that $\phi = \pi/2$ for small J_1 and $J_2 > 0$. This 90° coupling was first observed [110] in the transition regions between F-coupled and AF-coupled domains in an Fe/Cr wedge. A preponderance of evidence suggests that the BL–BQ model accurately describes Fe/Cr wedges. Azevedo *et al* [117] were able to use a single set of parameters including $\{J_1, J_2\}$ to fit BLS, MOKE, and FMR data. A similar feat was achieved by Grimsditch *et al* [118], who remarked that the sensitivity of J_2 to growth conditions implies that the BQ coupling is primarily extrinsic.

Following the extensive BLS and MOKE measurements [81] on Fe/Cr wedges summarized in figure 11, Heinrich *et al* [82] proposed the relation $J_2 \approx 0.1$ erg cm^{-2} + $0.16|J_1|$. Due to the agreement with the prediction [86] of the l–J model that $J_2 \approx 0.15|J_1|$, they argued that the second term in J_2 arises from the intrinsic contribution of a non-collinear SDW. Extrinsic contributions are held responsible for the dominant first term in J_2. The observed magnetic

saturation and the agreement between the MOKE and BLS measurements led Heinrich *et al* to conclude that Fe/Cr wedges are well described by the BL–BQ model. An inhomogeneous distribution of the exchange couplings can explain the two outstanding disagreements with the BL–BQ model: the absence of a kink in the MOKE signal at H_2 and the absence of a first-order jump at H_1, below which the Fe moments are antiparallel.

Many studies suggest that the thickness-fluctuation model [114] accurately describes the extrinsic part of J_2. Pierce *et al* [90] argue that the $1/N$ dependence of J_1 and the $1/N^2$ dependence of J_2 support equation (11) of the thickness-fluctuation model, as does the vanishing of J_2 near a phase slip [27]. Using a curved Cr single crystal with variable terrace length, Escorcia-Aparicio *et al* [119] confirmed that J_2 increases linearly with L_s as predicted by equation (11). Also in qualitative agreement with the thickness-fluctuation model, recent work by Hopster [120] on Fe/Cr bilayers indicates that rough regions of the Fe–Cr interface are BQ coupled below $T_{\rm N}^{\rm bulk}$ due to magnetic frustration.

But other measurements seem to conflict with the thickness-fluctuation model. The relative constancy of J_2 together with the growing oscillations of J_1 in figure 11 [81, 82] disagree with this model. The observed proportionality between J_1 and J_2 as a function of temperature [121, 122] also contradicts equation (11). In addition, the thickness-fluctuation model cannot explain some measurements on other trilayer systems [123–125].

Although the BL–BQ model is believed to correctly describe Fe/Cr trilayers, questions persist about the model appropriate to describe Fe/Cr multilayers. Recall that the torsion model requires $L_s < 100$ Å, which is satisfied in Fe/Cr multilayers but not in Fe/Cr wedges. Supported by the smooth evolution of the magnetization and the 50° coupling angle between Fe moments, Schreyer *et al* [23] argued that the torsion model applies to epitaxially grown Fe/Cr multilayers. As already remarked, an inhomogeneous distribution of the exchange coupling can explain [27, 82] the absence of a kink in the magnetization within the BL–BQ model. Nonetheless, the observed 50° coupling would require that $J_2 \approx 1$ erg cm^{-2}, which is about the same size as J_1. A far smaller value of J_2 was reported for Fe/Cr wedges, which, on the basis of the thickness-fluctuation model [114], would be expected to have a larger value of $J_2 \propto L_s$ than Fe/Cr multilayers.

The shorter terrace lengths of sputtered multilayers would seem to make that system more hospitable to the torsion model. As in the epitaxially grown multilayers, no kink was observed [26] in the magnetization of the sputtered system either above or below $T_{\rm N}^{\rm bulk}$. But the absence of a SDW in the region of strong BQ coupling indicates that the torsion model fails to describe sputtered multilayers.

4.3.3. The role of SDWs in the BQ coupling. One of the main arguments made in this paper has been that SDWs modify the BL exchange coupling J_1. What role if any do SDWs play in the BQ coupling J_2? Within the thickness-fluctuation model, a SDW indirectly affects the extrinsic BQ coupling through the dependence of J_2 on fluctuations of J_1. The small $0.16|J_1|$ contribution to J_2 found in BLS measurements [82] suggests that a SDW directly produces an intrinsic BQ coupling in Fe/Cr trilayers. However, more work is needed to verify that this term actually arises from the non-collinearity of a SDW for $H_1 < H < H_2$ or $0 < \Delta\phi < \pi$.

In epitaxially grown Fe/Cr multilayers, the most compelling evidence for the direct role of SDWs is the inability of the BL–BQ model to explain the observed 50° coupling [23]. Within the torsion model, the formation of H SDW domains can produce a coupling angle different from 90°. Unfortunately, the torsion model cannot explain the observed saturation of the Fe moments. We believe that thickness fluctuations are primarily responsible for the BQ coupling in both epitaxially grown and sputtered multilayers but that the formation of non-collinear SDW

domains in epitaxially grown multilayers allows the coupling angle ϕ to deviate from 90°. If, as predicted by Cornea and Stoeffler [87], non-collinear SDWs are replaced by collinear SDWs as the Fe moments become parallel ($\phi \to 0$), then the Fe moments would be torque-free and saturation could be achieved within such a hybrid model.

5. Open questions

As neutron-scattering measurements have made abundantly clear, the SDW phases of Fe/Cr multilayers are quite rich, with evidence for non-collinear phases that are absent in bulk Cr. One of the motivations of this review was to determine whether SDWs also affect the exchange coupling and magnetization. The introduction raised several questions about the role of SDWs. We return to those questions now.

5.1. Exchange coupling: what is the signature of a SDW?

Many properties of Fe/Cr trilayers and multilayers are also observed in systems with non-magnetic spacers. For example, a short-period IEC has also been found in Fe/Au [7], Co/Cu [8], and Fe/Ag [125] trilayers. Although interfacial interactions do induce a tiny [126,127], possibly non-collinear [128] spin modulation in non-magnetic spacers, a SDW instability is absent in all of these systems. So how does the presence of a SDW alter the short-period coupling?

Phenomenology [44–46] predicts that the short-period amplitude $D_{L,s}(T)$ falls off sharply above $T_{\mathrm{N}}^{\mathrm{bulk}}$. For a strained Cr spacer in an Fe/Cr wedge, this implies that $D_{L,s}(T)$ should drop off above about 230 K. On the other hand, the quantum-well model [14] predicts that $D_{L,s}(T)$ should fall off above the temperature $v_F/4\pi L \approx 1500\ \mathrm{K}/N$. These two temperature scales are the same for $N \approx 10$. But for $N \gg 10$, the predictions of the phenomenological and quantum-well models for $D_{L,s}(T)$ are quite different. As shown in figure 10(b), the rapid decay of the short-period coupling over a wide range of N above 300 K confirms the phenomenological model.

By far the most dramatic phenomenological predictions are for the temperature and thickness dependence of the short-period wavevector q_s in equation (5). According to the quantum-well model, q_s is given by the extremal, nesting wavevectors $Q_{\pm}$ of the bulk FS and should not depend strongly on temperature or thickness. But for $T < T_{\mathrm{N}}^{\mathrm{bulk}}$, phenomenology predicts that q_s jumps from $G/2$ to near $Q'_{\pm}$ after the first phase slip. For a fixed and large N, q_s is predicted to change from $Q'_{\pm}$ at $T_{\mathrm{N}}^{\mathrm{bulk}}$ to $G/2$ above T_{IC}. Since this behaviour is caused by the competition between I and C SDWs, it has no analogue in non-magnetic spacers. These predictions are strongly supported by the NIST measurements in figure 10(b).

Theoretically, SDWs also modify the thickness dependence of $D_{L,s}$. For a P spacer at $T = 0$, quantum-well models [12] dictate that $D_{L,s}$ falls off like $1/L$ when planes of the FS are nested. Below $T_{\mathrm{N}}^{\mathrm{bulk}}$, Fishman and Shi [46] predict that $D_{L,s} \sim 1/L^{1/2}$. But the first-principles calculations of van Schilfgaarde and Herman [71] indicate that $D_{L,s} \sim 1/L^0$ is independent of L in this case. Above $T_{\mathrm{N}}^{\mathrm{bulk}}$ but with a SDW still induced by the interfacial interactions, Fishman and Shi [46] predict that $D_{L,s} \sim 1/L^2$. Putting these details aside, it seems clear that because the SDW disappears with increasing L above $T_{\mathrm{N}}^{\mathrm{bulk}}$, $D_{L,s}$ must decay more rapidly above $T_{\mathrm{N}}^{\mathrm{bulk}}$ than below. By contrast, the long-period coupling is unaffected by the SDW [61] and is expected to decay like $1/L^2$ for all temperatures.

Due to small sample size, however, it is very difficult to experimentally determine the behaviour of $D_{L,s}$: for an 80 ML thick Fe/Cr wedge at room temperature, $J_{\mathrm{c}}(L)$ only passes through about four oscillations so only four data points are available to fit the dependence of $D_{L,s}$ on thickness. To make matters worse, the first two or three of those points may be

undermined by pre-asymptotic corrections [29, 30, 64]. Early experiments [6] found that H_2 falls off like $1/L$. Later measurements at NIST [90] could not distinguish whether $D_{L,s}$ decays like $1/L$ or $1/L^0$. Nevertheless, those measurements did verify that $D_{L,l}$ falls off more rapidly than $D_{L,s}$.

Almost every model predicts that the SDW enhances $D_{L,s}$. But here the comparison between theory and experiment is quite discouraging. Whereas several measurements [81, 121, 129] yields a maximum J_c of about 1 erg cm^{-2}, the predicted values (to convert between units, use 1 meV/a^2 = 1.93 erg cm^{-2}) are at least 15 times higher. These overestimates are made by tight-binding [17, 51], first-principles [19, 70–73], and phenomenological [44] calculations. While interfacial steps and Fe–Cr interdiffusion certainly suppress the short-period amplitude, the predicted coupling [17, 72] in realistic trilayers is still an order of magnitude too large.

Compare this to the case of trilayers with non-magnetic spacers. For Co/Cu trilayers, first-principles calculations [130] are in excellent agreement with measurements [8] not just for the IEC periods $2\pi/q_n$ but also for the phases ψ_n and amplitudes $D_{L,n}$. Quantum-well models for Co/Cu [131] predict coupling strengths only three times larger than the measured values. In Fe/Au wedges with very wide terraces [132], the observed short- and long-period amplitudes reach about 60% and 15% of the predicted values [133], respectively. The observed peak value of J_c at about 5 ML is approximately 0.4 erg cm^{-2} in Co/Cu [8] and 1.0 erg cm^{-2} in Fe/Au [132]. For comparison, the peak value in Fe/Cr [82] at 5 ML is about 0.8 erg cm^{-2}.

We must conclude that the agreement between experiment and theory is far worse for Fe/Cr trilayers than for trilayers with non-magnetic spacers. In large part, this may be caused by the sensitivity of the IEC to Fe–Cr interdiffusion [27]. Yet there is little indication that improved samples will ever yield a J_c that is 15 times larger than currently attainable [134]. So it may be worth re-examining the theoretical treatment of the SDW.

Recall that the SDW in bulk Cr is produced by fewer than half of the conduction electrons [36] and that the FS is only partially gapped below T_N^{bulk}. In a non-magnetic Cr spacer with $U = 0$, only electrons at the Fermi energy contribute to the IEC. The similar magnitudes of J_c in Fe/Cr and Fe/Au trilayers suggests that the exchange coupling lost by the partial gapping of the FS is compensated by the exchange coupling gained by the AF interaction between neighbouring Fe and Cr moments. This conclusion is supported by Mirbt *et al* [73], who found that the multiple scattering ($U = 0$) and SDW ($U > 0$) contributions to the exchange coupling are about equal. But it is unknown how the gapped and ungapped electrons cooperate to produce a single short-period coupling with a single wavevector and phase. To help resolve this question, photoemission measurements could be used to study the quantum-well states of the ungapped electrons in Fe/Cr trilayers.

5.2. Non-collinear SDWs and the torsion model: what are the requirements?

Although Schreyer *et al* [23, 24] observed H SDWs in epitaxially grown Fe/Cr multilayers, it is unclear whether these non-collinear SDWs can be described by the torsion model. In this subsection, we discuss the requirements for non-collinear SDWs and for the torsion model.

In a perfect trilayer, a non-collinear SDW first appears when the Fe moments deviate from CF conditions. Both tight-binding [84, 86, 115, 116] and phenomenological [88] models suggest that the non-collinear SDW remains stable under non-CF conditions only if the bulk C free energy is sufficiently lower than the bulk I free energy. If SDW nodes come at too small an energy cost, then the non-collinear state which first appears when $\Delta\phi$ deviates from 0 will disappear before the twist reaches $\Delta\phi = \pi$ [87]. In other words, the torsion model requires that the moment on every site should be fairly rigid and resist deformation.

Therefore, some of the most favourable systems for testing the predictions of the torsion model are Mn-based trilayers. Like Cr, Mn is also an itinerant antiferromagnet but the bulk SDW in γ-Mn alloys is always commensurate with a moment of $2.3\mu_B$ on every site [135,136]. In the magnetic multilayers discussed below, Mn forms a body-centred tetragonal structure that is unstable in bulk form [137].

Magnetization and FMR measurements performed [138] on $Fe_{0.25}Co_{0.75}$/Mn trilayers revealed a strong 90° coupling which may be described within the BL–BQ model by taking $J_1 \approx 0$ and $J_2 \approx 3.0$ erg cm^{-2}. To avoid such an enormous value for J_2 and to explain the observed gradual approach to saturation, Filipkowski *et al* concluded that the torsion model is more appropriate with $C_+ \approx C_- \approx 1.0$ erg cm^{-2}. Subsequent measurements [139] using soft x-ray magnetic circular dichroism confirmed the presence of a H SDW in the Mn spacer.

As discussed earlier, BLS measurements provide a powerful tool for discriminating between the BL–BQ and torsion models. Recall that BLS measurements [82] on Fe/Cr trilayers strongly supported the BL–BQ model. Based on the absence of magnetic saturation up to 10 kG, Chirita *et al* [140] argued that the torsion model better describes FeCo/Mn trilayers. Deviations from the predictions of equation (12) were explained by a twist of the moments within the FeCo layers.

Measurements on Fe/Mn wedges [137, 141] revealed a short-period oscillation in the strength of the 90° coupling between the Fe moments. The torsion model was used to fit MOKE results [141] with a single set of parameters $\{C_+, C_-\}$. By comparison, fitting those results to the BL–BQ model required a much wider range of parameters $\{J_1, J_2\}$ than warranted by the sample quality and by the clearly defined short-period coupling. Very recent STM and SEMPA measurements [142, 143] on Fe/Mn wedges also favour the torsion model. A generalized thickness-fluctuation model was invoked [143] to explain the small departures from the predictions of the torsion model.

Clearly, the evidence for the torsion model is much stronger in Mn-based trilayers than in epitaxially grown Fe/Cr multilayers. One might expect that the torsion model would be better suited to Fe/$Cr_{0.94}Fe_{0.06}$ multilayers where the CrFe spacer strongly favours a bulk C SDW. However, magnetization and resistivity measurements [144] on sputtered Fe/CrFe multilayers were unable to discriminate between the torsion and BL–BQ models.

5.3. Proximity to a bulk SDW instability: can it be detected?

At the start of this review, we posed the question 'If stranded on a desert island without neutron-scattering facilities but with BLS and MOKE apparatus available, could you detect a SDW in the spacer of a magnetic multilayer?' This review has shown that SDWs have several observable effects: the dramatic temperature dependence of the IEC wavevector and amplitude above the bulk Néel temperature, and in the case of BQ coupling, the gradual approach to saturation under an applied field. While the temperature dependence of the IEC wavevector has been definitely verified in Fe/Cr wedges, the decay of the IEC amplitude above T_N^{bulk} has been partially confirmed. However, there is little evidence that SDWs are primarily responsible for the BQ coupling of Fe/Cr multilayers.

A related question is whether the proximity to a SDW instability may be observed in a nearly perfect trilayer. First-principles calculations [73] indicate that a large spin modulation is induced in a Cr spacer with $U > 0$ even when the bulk SDW is unstable. So imagine that a P spacer with $U > 0$ is close to a SDW instability, which can be approached by either decreasing the FS mismatch or lowering the temperature.

Sufficiently close to the instability that a C SDW is induced throughout the spacer, the IEC will alternate between F and AF coupling without phase slips. When the temperature or

FS mismatch decreases below a threshold value, the first phase slip will appear for large N. After rapidly shifting to lower thickness, it will be followed by a series of regularly spaced phase slips which move closer together as the temperature or FS mismatch is lowered further. As T_N^{bulk} is approached, the amplitude $D_{L,s}(T)$ will increase rapidly.

The precise temperature or FS mismatch at which the SDW instability is reached may be difficult to determine. Certainly, the power p in the asymptotic behaviour of $D_{L,s} \sim 1/L^p$ is expected to change at T_N^{bulk}. But measuring p close to T_N^{bulk} would require a very thick Cr spacer. Since the pattern of phase slips will change continuously across T_N^{bulk}, it may in practice be impossible to determine whether the spacer material could support a bulk SDW (for large N) or is just close to a SDW instability.

I hope that this review has demonstrated that Fe/Cr trilayers and multilayers provide a unique testing ground for models of itinerant antiferromagnetism. Within the past decade alone, this system has given birth to GMR, oscillatory exchange coupling across metallic spacers, and the torsion model. The most surprising outcome of research into this system in the next decade will be if more surprises are not forthcoming.

Acknowledgments

The author would like to acknowledge correspondence and conversations with Drs Bret Heinrich, Dale Koelling, Daniel Pierce, Zhu-Pei Shi, Daniel Stoeffler, Richard Wood, and Hartmut Zabel. This research was sponsored by the US Department of Energy under contract DE-AC05-00OR22725 with Oak Ridge National Laboratory, managed by UT-Battelle, LLC.

References

[1] Grünberg P, Schreiber R, Pang Y, Brodsky M B and Sowers H 1986 *Phys. Rev. Lett.* **57** 2442
[2] Baibich M N, Broto J M, Fert A, Nguyen Van Dau F, Petroff F, Etienne P, Creuzet G, Friederich A and Chazelas J 1988 *Phys. Rev. Lett.* **61** 2472
[3] Binasch G, Grünberg P, Saurenbach F and Zinn W 1989 *Phys. Rev.* B **39** 4828
[4] Unguris J, Celotta R J and Pierce D T 1991 *Phys. Rev. Lett.* **67** 140
[5] Purcell S T, Folkerts W, Johnson M T, McGee N W E, Jager K, aan de Stegge J, Zeper W B, Hoving W and Grünberg 1991 *Phys. Rev. Lett.* **67** 903
[6] Barthélémy A, Fert A, Baibich M N, Hadjoudj S, Petroff F, Etienne P, Cabanel R, Lequien S, Nguyen Van Dau F and Creuzet G 1990 *J. Appl. Phys.* **67** 5908
[7] Fuss A, Demokritov S, Grünberg P and Zinn W 1992 *J. Magn. Magn. Mater.* **103** L221
[8] Johnson M T, Purcell S T, McGee N W E, Coehoorn R, aan de Stegge J and Hoving W 1992 *Phys. Rev. Lett.* **68** 2688
[9] Donath M, Scholl D, Mauri D and Kay E 1991 *Phys. Rev.* B **43** 13 164
[10] Parkin S S P, More N and Roche K P 1990 *Phys. Rev. Lett.* **64** 2304
[11] Wang Y, Levy P M and Fry J L 1990 *Phys. Rev. Lett.* **65** 2732
[12] Bruno P and Chappert C 1991 *Phys. Rev. Lett.* **67** 1602
Bruno P and Chappert C 1991 *Phys. Rev. Lett.* **67** 2592 (erratum)
Bruno P and Chappert C 1992 *Phys. Rev.* B **46** 261
[13] Slonczewski J C 1989 *Phys. Rev.* B **39** 6995
[14] Edwards D M, Mathon J, Muniz R B and Phan M S 1991 *Phys. Rev. Lett.* **67** 493
[15] Stiles M D 1993 *Phys. Rev.* B **48** 7238
[16] Stoeffler D and Gautier F 1990 *Prog. Theor. Phys. Suppl.* **101** 139
[17] Stoeffler D and Gautier F 1991 *Phys. Rev.* B **44** 10 389
[18] Fu C L and Freeman A J 1986 *J. Magn. Magn. Mater.* **54–57** 777
[19] Hirai K 1999 *J. Magn. Magn. Mater.* **198+199** 525
Hirai K 1999 *Phys. Rev.* B **59** R6612
[20] Niklasson A M N, Johansson B and Nordström L 1999 *Phys. Rev. Lett.* **82** 4544
[21] Unguris J, Celotta R J and Pierce D T 1992 *Phys. Rev. Lett.* **69** 1125

[22] Fawcett E 1988 *Rev. Mod. Phys.* **60** 209
Fawcett E, Alberts H L, Galkin V Yu, Noakes D R and Yakhmi J V 1994 *Rev. Mod. Phys.* **66** 25
[23] Schreyer A, Ankner J F, Zeidler Th, Zabel H, Schäfer M, Wolf J A, Grünberg P and Majkrzak C F 1995 *Phys. Rev.* B **52** 16 066
[24] Schreyer A, Ankner J F, Zeidler Th, Zabel H, Majkrzak C F, Schäfer M and Grünberg P 1995 *Europhys. Lett.* **32** 595
Schreyer A, Majkrzak C F, Zeidler Th, Schmitte T, Bödeker P, Theis-Bröhl K, Abromeit A, Dura J A and Watanabe T 1997 *Phys. Rev. Lett.* **79** 4914
[25] Fullerton E E, Bader S D and Robertson J L 1996 *Phys. Rev. Lett.* **77** 1382
[26] Adenwalla S, Felcher G P, Fullerton E E and Bader S D 1996 *Phys. Rev.* B **53** 2474
[27] Pierce D T, Unguris J, Celotta R J and Stiles M D 1999 *J. Magn. Magn. Mater.* **200** 290
[28] Zabel H 1999 *J. Phys.: Condens. Matter* **11** 9303
[29] Stiles M D 1999 *J. Magn. Magn. Mater.* **200** 322
[30] Bruno P 1999 *J. Phys.: Condens. Matter* **11** 9403
[31] Overhauser A W 1960 *Phys. Rev. Lett.* **4** 226
[32] Lomer W M 1962 *Proc. Phys. Soc.* **80** 489
[33] Fedders P A and Martin P C 1966 *Phys. Rev.* **143** 8245
[34] Loucks T L 1965 *Phys. Rev.* **139** A1181
[35] Fishman R S and Liu S H 1993 *Phys. Rev.* B **48** 3820
[36] Skriver H L 1981 *J. Phys. F: Met. Phys.* **11** 97
[37] Jiang X W and Fishman R S 1997 *J. Phys.: Condens. Matter* **9** 3417
Fishman R S, Jiang X W and Liu S H 1998 *Phys. Rev.* B **58** 414
[38] Sato H and Maki K 1973 *Int. J. Magn.* **4** 163
Sato H and Maki K 1974 *Int. J. Magn.* **6** 183
[39] Falicov L M and Penn D R 1967 *Phys. Rev.* **158** 476
[40] Barker A S Jr and Ditzenberger J A 1970 *Phys. Rev.* B **1** 4378
[41] Marcus P M, Qiu S-L and Moruzzi V L 1998 *J. Phys.: Condens. Matter* **29** 6541
[42] Mattson J, Brodsky M B, Ketterson J and You H 1990 *Mater. Res. Soc. Symp. Proc.* **160** 231
[43] Werner S A, Arrott A and Kendrick H 1967 *Phys. Rev.* **155** 528
[44] Shi Z-P and Fishman R S 1997 *Phys. Rev. Lett.* **78** 1351
[45] Fishman R S and Shi Z-P 1998 *J. Phys.: Condens. Matter* **10** L277
[46] Fishman R S and Shi Z-P 1999 *Phys. Rev.* B **59** 13 849
[47] See, for example,
Fetter A and Walecka J 1971 *Quantum Theory of Many-Particle Systems* (New York: McGraw-Hill) p 426
[48] Bödeker P, Hucht A, Schreyer A, Borchers J, Güthoff F and Zabel H 1998 *Phys. Rev. Lett.* **81** 914
[49] Berger A and Fullerton E E 1997 *J. Magn. Magn. Mater.* **165** 471
[50] Victora R H and Falicov L M 1985 *Phys. Rev.* B **31** 7335
[51] Hasegawa H 1990 *Phys. Rev.* B **42** 2368
Hasegawa H 1991 *Phys. Rev.* B **43** 10 803
[52] Yafet Y 1987 *Phys. Rev.* B **36** 3948
[53] Fry J L, Ethridge E C, Levy P M and Wang Y 1991 *J. Appl. Phys.* **69** 4780
[54] Shi Z-P, Levy P M and Fry J L 1992 *Phys. Rev. Lett.* **69** 3678
Shi Z-P, Levy P M and Fry J L 1994 *Europhys. Lett.* **26** 473
[55] Shi Z-P, Levy P M and Fry J L 1994 *Phys. Rev.* B **49** 15 159
[56] Ortega J E and Himpsel F J 1992 *Phys. Rev. Lett.* **69** 844
[57] Segovia P, Michel E G and Ortega J E 1996 *Phys. Rev. Lett.* **77** 3455
[58] Edwards D M, Mathon J and Muniz R B 1994 *Phys. Rev.* B **50** 16 066
[59] Tsetseris L, Lee B and Chang Y-C 1997 *Phys. Rev.* B **55** 11 586
[60] Fullerton E E, Conover M J, Mattson J E, Sowers C H and Bader S D 1993 *Phys. Rev.* B **48** 15 755
[61] Stiles M D 1996 *Phys. Rev.* B **54** 14 679
[62] Koelling D D 1994 *Phys. Rev.* B **50** 273
[63] Li D, Pearson J, Bader S D, Vescovo E, Huang D-J, Johnson P D and Heinrich B 1997 *Phys. Rev. Lett.* **78** 1154
[64] Costa A T Jr, d'Albuquerque e Castro J and Muniz R B 1999 *Phys. Rev.* B **59** 11 424
[65] Mathon J 1991 *J. Magn. Magn. Mater.* **100** 527
[66] Zhang Z, Zhou L, Wigen P E and Ounadjela K 1994 *Phys. Rev. Lett.* **73** 336
[67] Weinert M, Watson R E and Davenport J W 1985 *Phys. Rev.* B **32** 2115
[68] Kudrnovský J, Drchal V, Turek I and Weinberger P 1994 *Phys. Rev.* B **50** 16 105
Drchal V, Kudrnovský J, Turek I and Weinberger P 1996 *Phys. Rev.* B **53** 15 036

[69] Moruzzi V L and Marcus P M 1992 *Phys. Rev.* B **46** 3171
[70] Levy P M, Ounadjela K, Zhang S, Wang Y, Sommers C B and Fert A 1990 *J. Appl. Phys.* **67** 5914
[71] van Schilfgaarde M and Herman F 1993 *Phys. Rev. Lett.* **71** 1923
[72] Mirbt S, Skriver H L, Aldén M and Johansson B 1993 *Solid State Commun.* **88** 331
[73] Mirbt S, Niklasson A M N, Johansson B and Skriver H L 1996 *Phys. Rev.* B **54** 6382
[74] Grünberg P, Barnaś J, Saurenbach F, Fuss J A, Wolf A and Vohl M 1991 *J. Magn. Magn. Mater.* **93** 58
[75] Mattson J, Brumitt B, Brodsky M B and Ketterson J B 1990 *J. Appl. Phys.* **67** 4889
[76] Unguris J, Celotta R J, Tulchinsky D A and Pierce D T 1999 *J. Magn. Magn. Mater.* **198+199** 396
[77] Pierce D T, Unguris J, Celotta R J and Stiles M D 2001 *Physics of Low-Dimensional Systems* ed J L Moran-Lopez (New York: Plenum) at press
[78] Walker T G, Pang A W, Hopster H and Alvarado S F 1992 *Phys. Rev. Lett.* **69** 1121
[79] Turtur C and Bayreuther G 1994 *Phys. Rev. Lett.* **72** 1557
[80] Cochran J F 1997 *J. Magn. Magn. Mater.* **169** 1
[81] Heinrich B, From M, Cochran J F, Liao L X, Celinski Z, Schneider C M and Myrtle K 1993 *Mater. Res. Soc. Symp. Proc.* **313** 119
[82] Heinrich B, Cochran J F, Monchesky T and Urban R 1999 *Phys. Rev.* B **59** 14 520
Heinrich B, Cochran J F, Monchesky T and Urban R 2000 *J. Appl. Phys.* **87** 5449
[83] Hinchey L L and Mills D L 1986 *Phys. Rev.* B **33** 3329
[84] Stoeffler D and Gautier F 1993 *J. Magn. Magn. Mater.* **121** 259
[85] Freyss M, Stoeffler D and Dreyssé H 1997 *Phys. Rev.* B **56** 6047
[86] Stoeffler D and Gautier F 1993 *Magnetism and Structure in Systems of Reduced Dimension* ed R F C Farrow (New York: Plenum) p 411
[87] Cornea C and Stoeffler D 2000 *Europhys. Lett.* **49** 217
[88] Fishman R S 1999 *J. Appl. Phys.* **85** 5877
[89] Leng Q, Wolf J A, Grünberg P and Zinn W 1993 *Int. J. Mod. Phys.* B **7** 434
[90] Pierce D T, Stroscio J A, Unguris J and Celotta R J 1994 *Phys. Rev.* B **49** 14 564
[91] Venus D and Heinrich B 1996 *Phys. Rev.* B **53** R1733
[92] Heinrich B, Cochran J F, Venus D, Totland K, Atlan D, Govorkov S and Myrtle K 1996 *J. Appl. Phys.* **79** 4518
[93] Davies A, Stroscio J A, Pierce D T and Celotta R J 1996 *Phys. Rev. Lett.* **76** 4175
[94] Heinrich B, Cochran J F, Monchesky T and Myrtle K 1997 *J. Appl. Phys.* **81** 4350
[95] Petroff F, Barthélémy A, Hazmić A, Fert A, Etienne P, Lequien S and Creuzet G 1991 *J. Magn. Magn. Mater.* **93** 95
[96] Klautau A B, Legoas S B, Muniz R B and Frota-Pessôa S 1999 *Phys. Rev.* B **60** 3421
[97] Savage D E, Schimke N, Phang Y-H and Lagally M G 1992 *J. Appl. Phys.* **71** 3283
[98] Fishman R S 1998 *Phys. Rev.* B **57** 10 284
[99] Slonczewski J C 1995 *J. Magn. Magn. Mater.* **150** 13
[100] Fishman R S 1998 *Phys. Rev. Lett.* **81** 4979
[101] Bödeker P, Schreyer A and Zabel H 1999 *Phys. Rev.* B **59** 9408
[102] Schmitte T, Schreyer A, Leiner V, Siebrecht R, Theis-Bröhl K and Zabel H 1999 *Europhys. Lett.* **48** 692
[103] Fullerton E E, Riggs K T, Sowers C H, Bader S D and Berger A 1995 *Phys. Rev. Lett.* **75** 330
[104] Meersschaut J, Dekoster J, Schad R, Beliën P and Rots M 1995 *Phys. Rev. Lett.* **75** 1638
[105] Hill J P, Helgesen G and Gibbs D 1995 *Phys. Rev.* B **51** 10 366
[106] Sonntag P, Bödeker P, Schreyer A, Zabel H, Hamacher K and Kaiser H 1998 *J. Magn. Magn. Mater.* **183** 5
[107] Demuynck S, Meersschaut J, Dekoster J, Swinnen B, Moons R, Vantomme A, Cottenier S and Rots M 1998 *Phys. Rev. Lett.* **81** 2562
[108] Pflaum J, Pelzl J, Frait Z, Šturc P, Maryško M, Bödeker P, Theis-Bröhl K and Zabel H 1999 *J. Magn. Magn. Mater.* **198+199** 453
[109] Berger A and Hopster H 1994 *Phys. Rev. Lett.* **73** 193
[110] Rührig M, Schäfer R, Hubert A, Mosler R, Wolf J A, Demokritov S and Grünberg P 1991 *Phys. Status Solidi* a **125** 635
[111] Erickson R P, Hathaway K B and Cullen J R 1993 *Phys. Rev.* B **47** 2626
[112] Slonczewski J C 1993 *J. Magn. Magn. Mater.* **126** 374
[113] d'Albuquerque e Castro J, Ferreira M S and Muniz R B 1994 *Phys. Rev.* B **49** 16 062
[114] Slonczewski J C 1991 *Phys. Rev. Lett.* **67** 3172
[115] Freyss M, Stoeffler D and Dreyssé H 1996 *Phys. Rev.* B **54** R12 677
[116] Freyss M, Stoeffler D and Dreyssé H 1997 *J. Appl. Phys.* **81** 4363
[117] Azevedo A, Chesman C, Rezende S M, de Aguiar F M, Bian X and Parkin S S P 1996 *Phys. Rev. Lett.* **76** 4837
[118] Grimsditch M, Kumar S and Fullerton E E 1996 *Phys. Rev.* B **54** 3385

[119] Escorcia-Aparicio E J, Choi H J, Ling W L, Kawakami R K and Qiu Z Q 1998 *Phys. Rev. Lett.* **81** 2144
[120] Hopster H 1999 *Phys. Rev. Lett.* **83** 1227
[121] From M, Liao L X, Cochran J F and Heinrich B 1994 *J. Appl. Phys.* **75** 6181
[122] Heinrich B, Celinski Z, Cochran J F, Arrott A S, Myrtle K and Purcell S T 1993 *Phys. Rev.* B **47** 5077
Celinski Z, Heinrich B and Cochran J F 1995 *J. Magn. Magn. Mater.* **145** L1
[123] Gutierrez C J, Krebs J J, Filipkowski M E and Prinz G A 1992 *J. Magn. Magn. Mater.* **116** L305
Filipkowski M E, Gutierrez C J, Krebs J J and Prinz G A 1993 *J. Magn. Magn. Mater.* **73** 5963
[124] Rodmacq B, Dumesnil K, Mangin P and Hennion M 1993 *Phys. Rev.* B **48** 3556
[125] Unguris J, Celotta R J and Pierce D T 1993 *J. Magn. Magn. Mater.* **127** 205
[126] Samant M G, Stöhr J, Parkin S S P, Held G A, Hermsmeier B D, Herman F, van Schilfgaarde M, Duda L-C, Mancini D C, Wassdahl N and Nakajima R 1994 *Phys. Rev. Lett.* **72** 1112
[127] Niklasson A M N, Mirbt S, Skriver H L and Johansson B 1996 *Phys. Rev.* B **53** 8509
[128] Mathon J, Umerski A, Villeret M, Muniz R B and Edwards D M 2000 *J. Magn. Magn. Mater.* **217** 188
[129] Wolf J A, Leng Q, Schreiber R, Grünberg P A and Zinn W 1993 *J. Magn. Magn. Mater.* **121** 253
[130] Nordström L, Lang P, Zeller R and Dederichs P H 1994 *Phys. Rev.* B **50** 13 058
Lang P, Nordström L, Wildberger K, Zeller R, Dederichs P H and Hoshino T 1996 *Phys. Rev.* B **53** 9092
[131] Mathon J, Villeret M, Muniz R B, d'Albuquerque e Castro J and Edwards D M 1995 *Phys. Rev. Lett.* **74** 3696
Mathon J, Villeret M, Umerski A, Muniz R B, d'Albuquerque e Castro J and Edwards D M 1997 *Phys. Rev.* B **56** 11 797
[132] Unguris J, Celotta R J and Pierce D T 1997 *Phys. Rev. Lett.* **79** 2734
[133] Stiles M D 1996 *J. Appl. Phys.* **79** 5805
[134] Fert A, Grünberg P, Barthélémy A, Petroff F and Zinn W 1995 *J. Magn. Magn. Mater.* **140–144** 1
[135] Endoh Y and Ishikawa Y 1971 *J. Phys. Soc. Japan* **30** 1614
[136] Honda N, Tanji Y and Nakagawa Y 1976 *J. Phys. Soc. Japan* **41** 1931
[137] Purcell S T, Johnson M T, McGee N W E, Coehoorn R and Hoving W 1992 *Phys. Rev.* B **45** 13 064
[138] Filipkowski M E, Krebs J J, Prinz G A and Gutierrez C J 1995 *Phys. Rev. Lett.* **75** 1847
[139] Chakarian V, Idzerda Y U, Lin H-J, Gutierrez C J, Prinz G A, Meigs G and Chen C T 1996 *Phys. Rev.* B **53** 11 313
[140] Chirita M, Robins G, Stamps R L, Sooryakumar R, Filipkowski M E, Gutierrez C J and Prinz G A 1998 *Phys. Rev.* B **58** 869
[141] Yan S-S, Schreiber R, Voges F, Osthöver C and Grünberg P 1999 *Phys. Rev.* B **59** R11 641
[142] Tulchinsky D A, Unguris J and Celotta R J 2000 *J. Magn. Magn. Mater.* **212** 91
[143] Pierce D T, Davies A D, Stroscio J A, Tulchinsky D A, Unguris J and Celotta R J 2000 *J. Magn. Magn. Mater.* **222** 13
[144] Fullerton E E, Sowers C H and Bader S D 1997 *Phys. Rev.* B **56** 5468